
Taylor series expansion of the Ginzburg-Landau coefficients in the NJL model

Taylor-Entwicklung der Ginzburg-Landau Koeffizienten im NJL-Modell

Bachelor-Thesis von Robin Alexander Beck

Tag der Einreichung: 16. August 2019

1. Gutachten: Priv. Doz. Dr. Michael Buballa
2. Gutachten: Prof. Dr. Guy D. Moore



TECHNISCHE
UNIVERSITÄT
DARMSTADT

Department of Physics
Institute of Nuclear Physics
Nuclei, Hadrons and Quarks

Taylor series expansion of the Ginzburg-Landau coefficients in the NJL model
Taylor-Entwicklung der Ginzburg-Landau Koeffizienten im NJL-Modell

Vorgelegte Bachelor-Thesis von Robin Alexander Beck

1. Gutachten: Priv. Doz. Dr. Michael Buballa
2. Gutachten: Prof. Dr. Guy D. Moore

Tag der Einreichung: 16. August 2019

Abstract

In this thesis the location of the tricritical point (TCP) and critical endpoint (CEP) in the QCD phase diagram is investigated within a simple Nambu-Jona-Lasinio model (NJL) for the case of two-flavor quark matter. Applying the Ginzburg-Landau analysis for the grand thermodynamic potential with constituent mass M as order parameter in the chiral limit and also for a nonzero current quark mass determines exactly the TCP and CEP. Expanding the resulting Ginzburg-Landau coefficients $\alpha_n(T, \mu; M)$ through a Taylor series expansion at $\mu = 0$ leads to approximations of the critical points. In particular, the critical points in the NJL model are focused since the determined locations could be a useful estimation for similar expansions in lattice QCD. However, it is not clear yet which quantities are comparable to the Ginzburg-Landau coefficients.

Zusammenfassung

In dieser Arbeit wird die Lage des trikritischen Punkts und des kritischen Endpunkts im QCD Phasendiagramm im Rahmen eines einfachen Nambu-Jona-Lasinio-Modell (NJL) für den Fall von Zwei-Flavour Quark Materie untersucht. Durch Anwendung der Ginzburg-Landau Analyse für das großkanonische thermodynamische Potential mit Ordnungsparameter M im chiralen Limes sowie für nicht verschwindende Quarkmasse werden trikritischer Punkt und kritischer Endpunkt exakt bestimmt. Die Entwicklung der sich ergebenden Ginzburg-Landau Koeffizienten $\alpha_n(T, \mu; M)$ in einer Taylor-Reihe um $\mu = 0$ führt zu einer Approximation der kritischen Punkte. Insbesondere die kritischen Punkte im NJL-Modell stehen im Fokus der Arbeit, da die Bestimmung von dessen Positionen eine nützliche Näherung für ähnliche Entwicklungen innerhalb der QCD Gitterrechnungen sein könnten, wobei bislang nicht klar ist, welche Größe mit den Ginzburg-Landau Koeffizienten vergleichbar ist.

Contents

1	Introduction	3
----------	---------------------	----------

2	The Nambu-Jona-Lasinio model	6
2.1	The NJL Lagrangian	6
2.2	Gap equation	7
2.2.1	The integral $I(M)$ in the vacuum case	9
2.2.2	The integral $I(M)$ for nonzero temperature and chemical potential	10
2.3	Mean-field approximation	11
2.4	The thermodynamic potential	12
2.4.1	Behavior of the grand potential $\Omega_{NJL}(M)$	13
2.5	Solutions of the gap equation for zero chemical potential and zero temperature	16

3	Ginzburg-Landau analysis	19
3.1	The Ginzburg-Landau theory	19
3.2	Analysis in the chiral limit	20
3.2.1	The Ginzburg-Landau coefficients	21
3.2.2	Phase diagram with TCP	22
3.2.3	Constituent mass functions	23
3.3	Analysis for nonzero quark mass	24
3.3.1	The Ginzburg-Landau coefficients	25
3.3.2	Phase diagram with CEP	25
3.3.3	Constituent mass functions	26

4	Taylor series approximation of TCP and CEP	28
4.1	Approximation of the TCP	28
4.2	Approximation of the CEP	31
4.2.1	Constituent mass functions for the Taylor polynomials	34

5	Conclusion and outlook	36
----------	-------------------------------	-----------

1 Introduction

The quantum field theory which describes the fundamental physics of strong interaction between quarks and gluons is called quantum chromodynamics (QCD). The first formulation of this theory goes back to the 1970s and relates to the experimental confirmation that nucleons indeed consist of smaller particles. Therefore, the QCD describes quarks as main component of the nucleons, together with the gluons which occur as the corresponding interaction particles like the photons in quantum electrodynamics. In general, there exist six different flavors of quarks. Instead of an electric charge for the quarks, the theory deals with so called color charge. More specific, QCD is a non-abelian gauge theory with symmetry group $SU(3)$ due to the three possible quark colors red, green and blue. Especially the fact, that also gluons carry a color charge leads to an interaction between gluons themselves and makes the theory more complicated. Moreover, the color force between the components of a nucleon is responsible for the nuclear force which stick together the nucleus. The QCD is defined by the Lagrangian of the form

$$\mathcal{L}_{QCD} = \bar{\psi}(i\gamma^\mu D_\mu - \hat{m})\psi - \frac{1}{4}F_{\mu\nu}^a F^{a\mu\nu} \quad (1.1)$$

with the quark fields ψ and $\bar{\psi} = \psi^\dagger \gamma_0$ of six flavors $f = (u, d, s, c, b, t)$ and possible colors from $c = \{r, g, b\}$. Furthermore, the $\hat{m} = \text{diag}_f(m_u, m_d, m_s, m_c, m_b, m_t)$ denotes the mass matrix in flavor space and $F_{\mu\nu}^a$ is the gluon field strength tensor

$$F_{\mu\nu}^a = \partial_\mu A_\nu^a - \partial_\nu A_\mu^a + gf^{abc}A_\mu^b A_\nu^c \quad (1.2)$$

for the gluon field A_μ^a to which the quark fields are coupled by the covariant derivative

$$D_\mu = \partial_\mu - \frac{ig}{2}A_\mu^a \lambda^a \quad (1.3)$$

with Gell-Mann matrices λ^a , antisymmetric structure constants f^{abc} and g as QCD coupling constant [1].

One particular property of the QCD is the color confinement which states that unbound color charged particles could not be observed directly in the nature but only in a 'colorless' confinement. This means that under normal conditions quarks appear only in a special combination, the color neutral hadrons: Quark and antiquark with anticolor as mesons or three quarks with all three colors as baryons. The second important QCD property is the asymptotic freedom that results in a vanishing coupling constant for high energies and very strongly confined interactions in the low energy scale. For high energies, i.e. at a high temperature or density, the hadrons must overlap so strongly that they are not individual anymore. Thus, the quarks and gluons get deconfined and form the so called quark-gluon plasma (QGP) which is the focus of several experimental investigations at heavy ion colliders like at CERN or GSI. Natural occurrence of the QGP is suspected in the dense center of neutron stars

but surely it appeared in the early universe at the high temperatures directly after the Big Bang.

Special interest of experimental and theoretical physicists lies on the investigation of the phase transition between the confined hadronic phase and the QGP. For this reason, the QCD phase diagram which illustrates the different phases of quarks at given chemical potential and temperature is studied. A really simplified QCD phase diagram contains only one phase boundary that separates the area of confined quarks at low temperatures and chemical potentials from the QGP, such that both phases are in equilibrium at the boundary. In particular, one can think of more detailed phase diagrams containing a first order phase boundary that ends at a point called critical endpoint (CEP) where the phase transition is of second order. An example of such a qualitative phase diagram is shown in figure 1.1.

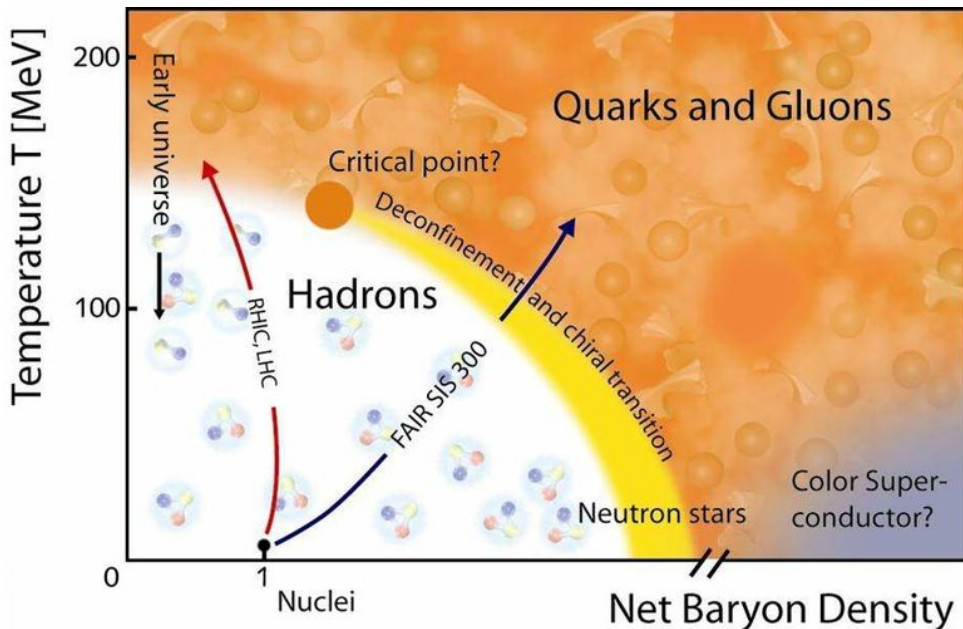


Figure 1.1: Schematic illustration of a simple QCD phase diagram with QGP, CEP, hadronic phase and crossover area taken from [2]. Note: The diagram shows the relation of temperature over density such that there is a finite area for the phase transition corresponding to a strict phase boundary line in case of temperature over chemical potential.

A famous non-perturbative approach to QCD is the lattice QCD that uses a discrete set of spacetime points for a simplified numerical calculation of the occurring path integrals. This approach is often used for investigations of the QCD phase diagram at high temperatures, however, there is a so called sign problem due to the fermions such that an analysis at non-vanishing chemical potentials is not possible. Hence, other methods like effective models such as the Nambu-Jona-Lasinio (NJL) or quark-meson (QM) model as well as a Taylor series expansion of the grand canonical potential at chemical potential $\mu = 0$ must be used for a deeper analysis of possible phase transitions and the location of the critical endpoint.

In this work the QCD phase diagram will be analyzed within the effective NJL-model for two-flavor quark matter that already provides the essential phenomenon of chiral symmetry breaking and allows calculations with non-vanishing chemical potentials. For this, the Ginzburg-Landau analysis will be applied for determining the location of the critical and tricritical point as well as the second order phase boundary in the chiral limit, i.e. for zero quark mass. Furthermore, the expansion of the resulting Ginzburg-Landau coefficients in a Taylor series will lead to an approximation of TCP and CEP which will be discussed with regard to the possibilities of other physical quantities in Taylor series expansions.

First, this work will start with an introduction to the NJL model and the corresponding Lagrangian with its symmetries in the second chapter, where special emphasis lies on deriving an expression for the thermodynamic potential. In chapter three, the method of Ginzburg-Landau will be developed to investigate the phase diagram with its critical endpoint. Afterwards, the chapter makes use of the introduced method within a Ginzburg-Landau analysis of the derived thermodynamic potential with constituent mass M as order parameter. Then, in the fourth chapter a Taylor series expansion at vanishing chemical potential is applied to make an approximation of the exact determined location of the TCP in the chiral limit and the CEP for finite bare mass. Finally, the results and the obtained approximation will be discussed in the last chapter together with a short outlook.

2 The Nambu-Jona-Lasinio model

The origin of the Nambu-Jona-Lasinio model goes back to two papers by Y. Nambu and G. Jona-Lasinio in 1961 about the dynamical mass generation for nucleons [3, 4]. The great idea was, that they developed the model analogous to the construction of Cooper pairs in the BCS theory of superconductivity such that it describes the nucleon-nucleon interaction. Indeed, this model was invented before quarks and QCD were known, such that the concept of color charge is not included in the NJL model. Moreover, the two QCD properties of asymptotic freedom and confinement are not covered through the NJL Lagrangian. Nevertheless, the model has been reinterpreted as low energy effective theory for QCD since the chiral symmetry of the strong interaction is reflected very well. In many problems, chiral symmetry is the important feature to study, for instance pions can be explained as Goldstone bosons of the spontaneous chiral symmetry breaking. The so-called color superconductivity is another field of application where the NJL model is very useful but which is not discussed in this work. In case of using the original Lagrangian of the NJL model one has to deal with nucleonic fields instead of the quark fields.

2.1 The NJL Lagrangian

This thesis will restrict to a simple form of the NJL model with quark fields of two flavors and three color degrees of freedom. Instead of gluon exchange, the strong interaction is given through terms of scalar-isoscalar and pseudoscalar-isovector four-point interactions. The corresponding NJL Lagrangian density is given as follows

$$\mathcal{L}_{NJL} = \bar{\psi}(i\cancel{D} - \underline{m})\psi + G \left[(\bar{\psi}\psi)^2 + (\bar{\psi}i\gamma_5\vec{\tau}\psi)^2 \right] \quad (2.1)$$

with the $3 + 1$ dimensional Dirac spinors ψ and $\bar{\psi} = \psi^\dagger\gamma_0$ for the quark and anti quark fields with $N_f = 2$ flavors and $N_c = 3$ colors. Therefore, one has to deal in total with $4N_fN_c$ components. The Pauli matrices in isospin space are denoted by $\vec{\tau}$ and the expression $\underline{m} = \text{diag}(m_u, m_d)$ is the bare mass matrix in flavor space containing the masses of up and down quark. However, in the following the bare quark masses will assumed to be degenerate, i.e. $m \equiv m_u = m_d$, since they are nearly the same compared to the corresponding hadron masses. The first part of the Lagrangian is the free Dirac field which leads to the Dirac equation. The second term corresponds to the four-point interaction and consists of a scalar $(\bar{\psi}\psi)$ and pseudoscalar $(\bar{\psi}i\gamma_5\vec{\tau}\psi)$ term. The scalar coupling constant for the interaction is G . Because of the four-point interaction, the NJL model cannot be renormalized. Further, the occurrence of divergent integrals leads to a regularisation in the concrete calculations later on [5].

The important property of the stated NJL Lagrangian lies behind the common symmetries with QCD [6]. Starting with the most general symmetry, the Lagrangian is invariant under global $U(1)_V$ phase transformation given by

$$\psi \rightarrow \exp(-i\alpha)\psi \quad \text{and} \quad \bar{\psi} \rightarrow \bar{\psi} \exp(i\alpha) \quad (2.2)$$

for a $\alpha \in \mathbb{R}$. According to Noether's theorem this transformation results in the conservation of the baryon number. Second, there is an invariance under a vector $SU(2)_V$ transformation due to the assumption of equal quark masses m . The transformation is given by

$$\psi \rightarrow \exp\left(-\frac{i}{2}\vec{\theta}\vec{\tau}\right)\psi \quad \text{and} \quad \bar{\psi} \rightarrow \bar{\psi} \exp\left(\frac{i}{2}\vec{\theta}\vec{\tau}\right) \quad (2.3)$$

with $\vec{\theta} \in \mathbb{R}^3$ and results in the conservation of isospin. Third, the unitary axial transformation

$$\psi \rightarrow \exp\left(-\frac{i}{2}\gamma_5\vec{\theta}\vec{\tau}\right)\psi \quad \text{and} \quad \bar{\psi} \rightarrow \bar{\psi} \exp\left(-\frac{i}{2}\gamma_5\vec{\theta}\vec{\tau}\right) \quad (2.4)$$

with $\vec{\theta} \in \mathbb{R}^3$ lets the Lagrangian invariant. These $SU(2)_A$ axial transformations do not form a group. Instead, considering the latter two transformations together one gets the group $\mathcal{S}_{chiral} = SU(N_f)_L \times SU(N_f)_R = SU(2)_V \times SU(2)_A$ which is known as chiral symmetry. Chirality describes a phenomenon that is not identical to its mirror image. For example, the spin of a particle defines a helicity or handedness such that chirality is a conserved property for particles with zero mass. Since the NJL Lagrangian is not invariant under $SU(2)_A$ transformations in the case of nonzero bare mass m the chiral symmetry is explicit broken. This is due to the term $\bar{\psi}m\psi$ in the free Dirac part. Furthermore, the chiral symmetry is spontaneously broken in the chiral limit $m \rightarrow 0$ which will be an important characteristics of the NJL model for the following investigations. The spontaneous chiral symmetry breaking corresponds to a Goldstone boson with zero mass in the chiral limit. However, explicit symmetry breaking is indicated by a Goldstone boson with finite mass, the pion. Altogether the NJL model has the symmetry of the form

$$\mathcal{S}_{NJL} = SU(2)_V \times SU(2)_A \times U(1)_V \quad (2.5)$$

which includes \mathcal{S}_{chiral} and coincides with the QCD symmetries such that \mathcal{L}_{QCD} approximately satisfies this in the case of small equal masses. It should be said that in a classical sense the QCD Lagrangian in the limit of massless quarks is also invariant under a global axial transformation $U(1)_A$ given through

$$\psi \rightarrow \exp(i\alpha\gamma_5)\psi \quad \text{and} \quad \bar{\psi} \rightarrow \bar{\psi} \exp(i\alpha\gamma_5) \quad (2.6)$$

with $\alpha \in \mathbb{R}$. Since this symmetry is broken on the quantum level it is not seen as real for QCD and hence not considered in the following.

2.2 Gap equation

The aim of this section is the derivation of an expression for the effective quark mass which exists due to the interactions terms of the effective theory. Starting with a single quark of current or bare quark mass m the

coupling to itself in the scalar and pseudoscalar channel of the NJL Lagrangian leads to the quark self-energy. This self-energy in turn shifts the quark mass and results in the effective mass that is also called constituent quark mass and will be denoted by M . Through calculations of the self-energy in Hartree approximation the corresponding self-consistency equation, the Dyson equation, can be obtained [7]. This equation describes the propagation of quarks with 'dressed' mass M in relation to quarks with 'bare' mass m . Hence, the corresponding Feynman propagators as the typical fermionic propagators with their respective masses will be considered first [8, 9]. Together with the Feynman rules this yields the bare propagator for a quark with momentum p and mass m

$$iS_0(p) = i \frac{\not{p} + m}{p^2 - m^2 + i\epsilon} \quad (2.7)$$

as well as the appropriate dressed quark propagator which is the same with constituent quark mass M :

$$iS(p) = i \frac{\not{p} + M}{p^2 - M^2 + i\epsilon} \quad (2.8)$$

Writing the self-energy Σ as a real quantity, it can be related to the propagators by directly plugging in the expressions into the Dyson equation through

$$iS(p) = iS_0(p) + iS_0(p)(-i\Sigma)iS(p). \quad (2.9)$$

The self-consistency equation can be viewed also in a diagrammatic way in figure 2.1.

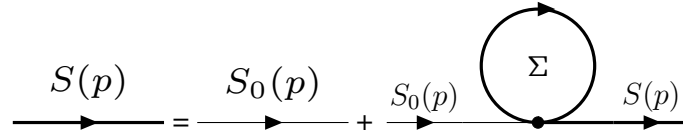


Figure 2.1: Diagrammatic form of the Dyson equation for the dressed (bold) and bare (thin) quark propagator, containing a loop for the self-energy contribution.

For an explicit expression of the self-energy, the sum of the outer products of each interaction must be calculated. Moreover, an integration over the momentum k of the loop for the dressed propagator takes place. All in all, it states

$$\begin{aligned} \Sigma &= 2G \left[\mathbb{1} \int \frac{d^4k}{(2\pi)^4} \text{Tr} [\mathbb{1} iS(k)] + i\gamma_5 \tau_a \int \frac{d^4k}{(2\pi)^4} \underbrace{\text{Tr} [i\gamma_5 \tau_a iS(k)]}_{=0} \right] \\ &= 2Gi \int \frac{d^4k}{(2\pi)^4} \frac{1}{k^2 - M^2 + i\epsilon} \text{Tr} [\gamma^\mu k_\mu + M] \\ &= 2Gi \int \frac{d^4k}{(2\pi)^4} \frac{1}{k^2 - M^2 + i\epsilon} N_f N_c 4M \\ &=: 8GN_f N_c MI(M) \end{aligned} \quad (2.10)$$

where the fact is used that traces of Pauli and odd numbers of gamma matrices disappear. Formally, the occurring traces have to be evaluated in Dirac, color and flavor space. Thus, the trace of the unit matrix is evaluated to the factor $4N_f N_c$ due to the color and flavor degeneracy. Multiplying the Dyson equation 2.9 from

the left and right side with the inverse of the propagators leads to an equivalent expression for the constituent quark mass:

$$\begin{aligned}
S_0^{-1}(p) &= S^{-1}(p) + \Sigma \\
\Leftrightarrow \not{p} - m &= \not{p} - M + \Sigma \\
\Leftrightarrow M &= m + 8GN_f N_c M I(M)
\end{aligned} \tag{2.11}$$

The equation in the last step is often called the gap equation since it allows non-trivial constituent masses $M \neq m$ as solution which on the other hand produces a gap of $\Delta E = 2M$ in the quark spectrum. Often, the mass which minimizes the vacuum energy is searched. Especially, the evaluation of the integral

$$I(M) = i \int \frac{d^4 k}{(2\pi)^4} \frac{1}{k^2 - M^2 + i\epsilon} \tag{2.12}$$

is important for finding the right solutions of the gap equation. The given integral 2.12 is in the vacuum case where the residue theorem is applied, however, in cases where already finite temperatures and chemical potentials play a role, the integral gets modified by the Matsubara formalism.

2.2.1 The integral $I(M)$ in the vacuum case

For zero temperature and chemical potential the integral $I(M)$ can be rewritten first with aid of the single particle energy $E_{\vec{k}} \equiv \sqrt{\vec{k}^2 + M^2}$. Furthermore, a factorization of the denominator is applied before the residue theorem can be used:

$$\begin{aligned}
I(M) &= i \int \frac{d^3 k}{(2\pi)^3} \int \frac{dk_0}{2\pi} \frac{1}{k_0^2 - E_{\vec{k}}^2 + i\epsilon} \\
&= i \int \frac{d^3 k}{(2\pi)^3} \int \frac{dk_0}{2\pi} \underbrace{\frac{1}{k_0 + E_{\vec{k}} - i\epsilon'} \cdot \frac{1}{k_0 - E_{\vec{k}} + i\epsilon'}}_{= \lim_{\epsilon \rightarrow 0} \frac{1}{2\pi} \cdot \frac{2\pi i}{-E_{\vec{k}} - E_{\vec{k}} + 2i\epsilon'}} \\
&= \int \frac{d^3 k}{(2\pi)^3} \frac{1}{2E_{\vec{k}}} \\
&= \frac{1}{4\pi^2} \int_0^\infty dk \frac{k^2}{E_{\vec{k}}}
\end{aligned} \tag{2.13}$$

where the infinitesimal quantity $\epsilon' = \frac{\epsilon}{2E_{\vec{k}}}$ is rescaled (ϵ'^2 is neglected) and spherical coordinates are taken for simplifying the expression in the last step. The residue theorem is applied for the k_0 -integration with a semicircle in the upper complex half plane as appropriate integration contour that contains only the shifted pole $k_0 = -E_{\vec{k}} + i\epsilon'$. Certainly, the final term obtained for the integral is divergent and since the NJL model is also non-renormalizable, a sort of regularisation scheme must be used for ending up with a finite value. Commonly, all regularisation schemes apply a special cut-off parameter Λ which is chosen in such a way that the model reproduces the correct results for well known properties of some particles.

For instance, one can work with the pion decay constant and pion mass in vacuum. In the given case a sharp 3-momentum cut-off will be taken as scheme. The idea is to bound the upper integral limit by restricting the absolute value of the momentum to values $k \leq \Lambda$ smaller than the cut-off, for example

$$\int_0^\infty d^3k f(\vec{k}) \rightarrow \int_0^\Lambda d^3k f(\vec{k}) \quad (2.14)$$

for a function f with divergent integral. The main advantage of this method is a possible analytically solvable integral at the end, though the scheme breaks the Lorentz invariance. For the considered integral, one can make use of this advantage and obtains the following analytic expression:

$$I(M) = \frac{1}{4\pi^2} \int_0^\Lambda dk \frac{k^2}{\sqrt{\vec{k}^2 + M^2}} = \frac{1}{8\pi^2} \left[\Lambda \sqrt{\Lambda^2 + M^2} - M^2 \operatorname{arsinh} \left(\frac{\Lambda}{M} \right) \right] \quad (2.15)$$

Together with this result, the effective mass solution of the gap equation can be found. Therefore, the parameters of the model must be fixed and the value of the cut-off has to be determined suitable. Concrete values and the parameter choice will be given later with some numerical results.

2.2.2 The integral $I(M)$ for nonzero temperature and chemical potential

The main purpose is to study the phase transitions and the critical endpoint in the phase diagram and therefore it is necessary to evaluate the quark loop in the gap equation at finite temperatures and chemical potentials. That means the integral $I(M)$ is considered in medium where the framework of a thermal field theory, the Matsubara formalism, is applied [10]. There, one sums over discrete imaginary frequencies, the so-called Matsubara frequencies, such that the energy-integration is replaced. Then, the integral can be written with the substitution

$$i \int \frac{d^4k}{(2\pi)^4} f(k) \rightarrow -T \sum_n \int \frac{d^3k}{(2\pi)^3} f(i\omega_n + \mu, \vec{k}) \quad (2.16)$$

where $\omega_n = (2n + 1)\pi T$ with $n \in \mathbb{Z}$ denote the fermionic Matsubara frequencies. By that, one obtains an integral depending also on T and μ besides the constituent mass M which leads to the notation for the medium $I_{med}(M) \equiv I(T, \mu, M)$. An analytical simplification of the expression is started with a partial fraction decomposition:

$$\begin{aligned} I_{med}(M) &= -T \sum_n \int \frac{d^3k}{(2\pi)^3} \frac{1}{(i\omega_n + \mu)^2 - E_{\vec{k}}^2} \\ &= \int \frac{d^3k}{(2\pi)^3} \frac{1}{2E_{\vec{k}}} \left[-T \sum_n \left(\frac{1}{i\omega_n + \mu - E_{\vec{k}}} - \frac{1}{i\omega_n + \mu + E_{\vec{k}}} \right) \right] \end{aligned} \quad (2.17)$$

Further, a double use of the residue theorem is necessary to receive the right integral form. It starts with a conversion of the Matsubara frequencies sum into an integral, using the residue theorem backwards. For this reason, an auxiliary function with poles at the Matsubara frequencies with residue $-T$ is introduced.

That leads to the following expression:

$$\begin{aligned}
I_{med}(M) &= \int \frac{d^3k}{(2\pi)^3} \frac{1}{2E_{\vec{k}}} \frac{1}{2\pi i} \int_C dz \frac{1}{1 + e^{\frac{z}{T}}} \left(\frac{1}{z + \mu - E_{\vec{k}}} - \frac{1}{z + \mu + E_{\vec{k}}} \right) \\
&= \int \frac{d^3k}{(2\pi)^3} \frac{1}{2E_{\vec{k}}} - \int \frac{d^3k}{(2\pi)^3} \frac{1}{2E_{\vec{k}}} \left(\frac{1}{1 + \exp\left(\frac{E_{\vec{k}} - \mu}{T}\right)} + \frac{1}{1 + \exp\left(\frac{E_{\vec{k}} + \mu}{T}\right)} \right)
\end{aligned} \tag{2.18}$$

In the last step, the integration contour in the complex plane is deformed analogous to [11] and afterwards the residue theorem is used as usual for the integration around the two poles $z_{1/2} = \pm E_{\vec{k}} - \mu$ as depicted in figure 2.2. The final result consists of the vacuum integral in the first part and a contribution which can be identified as terms of quark and antiquark occupation numbers due to the Fermi-Dirac distribution:

$$n_k(T, \mu) = \frac{1}{1 + \exp\left(\frac{E_{\vec{k}} - \mu}{T}\right)} \quad \text{and} \quad \bar{n}_k(T, \mu) = \frac{1}{1 + \exp\left(\frac{E_{\vec{k}} + \mu}{T}\right)} \tag{2.19}$$

The two results differ only in the sign of the quark chemical potential which is an indication of the charge symmetry.

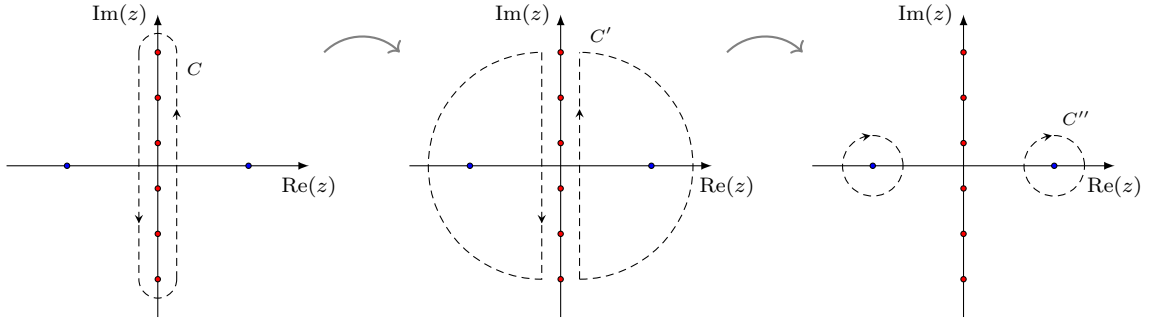


Figure 2.2: Transformation of the integration contour from left to right of the integral $I_{med}(M)$. The poles are indicated by small red (imaginary) and blue (real) dots.

To sum it all up, the following representation of the integral $I(M)$ was derived in this section:

$$I_{med}(M) = \int \frac{d^3k}{(2\pi)^3} \frac{1}{2E_{\vec{k}}} [1 - n_k - \bar{n}_k] \tag{2.20}$$

Putting this result inside the gap equation 2.11 yields a relation for the constituent mass $M(T, \mu)$ which is a function of temperature and chemical potential then.

2.3 Mean-field approximation

The results of the previous sections led to an formulation of the gap equation for vacuum and medium case that can be solved for the constituent mass M . Commonly, finding a stable constituent mass is related to the minimization problem for the thermodynamic potential. In order to calculate the latter, a mean-field approximation is considered. That means the Lagrangian will be linearized for simplification of the occurring functional integral. To this end, the interaction terms must be expanded around the expectation values of the quark fields.

The expectation value of $\bar{\psi}\psi$ yields an expression that is referred to as chiral or quark condensate and which is closely related to the constituent mass. For the quark condensate it holds

$$\begin{aligned}\langle\bar{\psi}\psi\rangle &= -i \int \frac{d^4k}{(2\pi)^4} \text{Tr} [S(k)] \\ &= -\frac{M-m}{2G}\end{aligned}\quad (2.21)$$

where the equality follows directly from the gap equation 2.11 with the corresponding expression for the self-energy 2.10. For the expansion around the expectation one writes $\bar{\psi}\psi = \langle\bar{\psi}\psi\rangle + \delta(\bar{\psi}\psi)$. Since the interaction term appears squared in the Lagrangian, the expansion result can be squared too with substituting the remaining δ term by terms of the original expression itself:

$$(\bar{\psi}\psi)^2 \approx \langle\bar{\psi}\psi\rangle^2 + 2\langle\bar{\psi}\psi\rangle\delta(\bar{\psi}\psi) = 2\langle\bar{\psi}\psi\rangle(\bar{\psi}\psi) - \langle\bar{\psi}\psi\rangle^2 \quad (2.22)$$

For this approximation the quadratic fluctuation term $\delta(\bar{\psi}\psi)^2$ is omitted. The same procedure can be carried out for the pseudo-scalar interaction but this will lead to a vanishing expectation value due to the fact that it still holds $\text{Tr} [i\gamma_5\tau_a S(k)] = 0$ as in the equations of 2.10. That means that only the condensate from the scalar interaction will be treated since the one from the pseudoscalar interaction is seen as vanishing within the scope of this work. Inserting the results of the mean-field approximation (MF), the Lagrangian can be expressed in terms of the quark condensate by

$$\begin{aligned}\mathcal{L}_{NJL} &\approx \bar{\psi}(i\cancel{\partial} - m)\psi + G \left(\langle\bar{\psi}\psi\rangle (\bar{\psi}\psi) - \langle\bar{\psi}\psi\rangle^2 \right) \\ &= \bar{\psi} \left(i\cancel{\partial} - \underbrace{(m - 2G\langle\bar{\psi}\psi\rangle)}_{=M} \right) \psi - G \langle\bar{\psi}\psi\rangle^2\end{aligned}\quad (2.23)$$

where the interaction part is absorbed in the introduced effective mass term $M = m - 2G\langle\bar{\psi}\psi\rangle$. Finally, the effective mass can be used for rewriting the Lagrangian once again which results in the form of a free quark with mass M in an effective potential:

$$\mathcal{L}_{NJL}^{MF} = \bar{\psi}(i\cancel{\partial} - M)\psi - \frac{(M-m)^2}{4G} \quad (2.24)$$

The second term must not be dropped because there the dependence of the constituent mass M is included.

2.4 The thermodynamic potential

The linearized Lagrangian \mathcal{L}_{NJL}^{MF} in 2.24 will be used for the thermodynamic potential which describes the system. This is important since then further thermodynamic quantities for studying the chiral symmetry breaking can be derived. For this, it is typical to work with the grand canonical potential due to the varying number of particles that should not be limited for fixed temperature and chemical potential. According to statistical physics, the grand potential can be obtained through a relation with the partition function denoted by \mathcal{Z} and the inverse temperature $\beta = \frac{1}{T}$.

This relation is given in the following way:

$$\Omega = -\frac{1}{\beta V} \ln (\mathcal{Z}) \quad (2.25)$$

Moreover, it is familiar that the partition function for a grand canonical ensemble, which is quantum mechanical and discrete, can be written as the trace of the Boltzmann factor. In the given case, it holds

$$\mathcal{Z} = \text{Tr} \left[e^{-\beta(H-\mu N)} \right] \quad (2.26)$$

where strictly speaking the partition function depends on μ and T . Here, the Hamilton operator $H = \int d^3x \mathcal{H}$, defined through a Hamilton density \mathcal{H} , and the total quark number operator $N = \int d^3x \bar{\psi}\psi$ appear. Next, the trace can be transformed into a functional integral for the partition function

$$\mathcal{Z} = \int \mathcal{D}\bar{\psi}\mathcal{D}\psi \exp \left\{ - \int_{[0,\beta] \times V} d^4x (\mathcal{L}_E - \mu \mathcal{N}) \right\} \quad (2.27)$$

considered in the Euclidian space $x = (\tau, \vec{x})$ with imaginary time $\tau = it$. Further, \mathcal{L}_E is the corresponding Euclidian Lagrangian from \mathcal{L}_{NJL}^{MF} with imaginary time and \mathcal{N} the particle density. Starting from this, the grand potential can be obtained together with equation 2.25 by a long calculation analogous to [10] which is not discussed in detail here. In the end, the mean-field grand potential for the Nambu-Jona-Lasinio model is given by:

$$\begin{aligned} \Omega_{NJL}(T, \mu; M) = & \frac{(M-m)^2}{4G} - 2N_f N_c \frac{4\pi}{(2\pi)^3} \left\{ \int_0^\Lambda dk k^2 E_{\vec{k}} \right. \\ & \left. + \int_0^\infty dk k^2 T \left[\ln \left(1 + \exp \left(-\frac{E_{\vec{k}} - \mu}{T} \right) \right) + \ln \left(1 + \exp \left(-\frac{E_{\vec{k}} + \mu}{T} \right) \right) \right] \right\} \end{aligned} \quad (2.28)$$

The potential consists of a M -dependent term from the Lagrangian in the front and the free quark gas contribution which in turn consists of the zero-point energy term from the vacuum and the medium part with quark and antiquark contribution, noticeable due to the different sign of the chemical potential. The pre-factor $2N_f N_c \frac{4\pi}{(2\pi)^3}$ is a result of spin, flavor and color degeneracy as well as the factors from the spherical integral in momentum space. To the expression of the potential one can also add any constant which would not change the associated physics. For the divergent first integral, describing the vacuum contribution, a regularization through the 3-momentum cut-off as in example 2.14 is applied. Since the second integral is convergent, there is no cut-off necessary for the calculations.

2.4.1 Behavior of the grand potential $\Omega_{NJL}(M)$

The derived thermodynamic potential gives rise to the condition $\frac{\partial \Omega_{NJL}}{\partial M} = 0$ for finding effective masses M which leads to extrema of the potential. One can show, that this condition is equivalent to the gap equation 2.11. Thus, searching for solutions of the obtained condition is a rational criterion for the correct masses. Though, only the constituent mass corresponding to the global minimum of the grand potential is the stable mass. For this reason, the next step is to investigate the behavior of the potential $\Omega_{NJL}(M)$ as function of

the constituent mass. The two cases of a nonzero current quark mass and the chiral limit with $m = 0$ will be compared. Therefore, an appropriate set of parameters for the used regularization scheme is necessary. For the course of this work the following parameters will be used:

$$G = 2.44\Lambda^2, \quad \Lambda = 587.9 \text{ MeV} \quad \text{and} \quad m = 5.6 \text{ MeV} \quad (2.29)$$

These parameters originate from [7] where they were determined by fitting them to proper values for the pion mass $m_\pi = 135 \text{ MeV}$, the pion decay constant $f_\pi = 92.4 \text{ MeV}$ and the quark condensate $\langle \bar{\psi}\psi \rangle^{1/3} = -240.8 \text{ MeV}$ in the vacuum. First, the shape of the thermodynamic potential is considered for points along the T -axis and afterwards along the μ -axis.

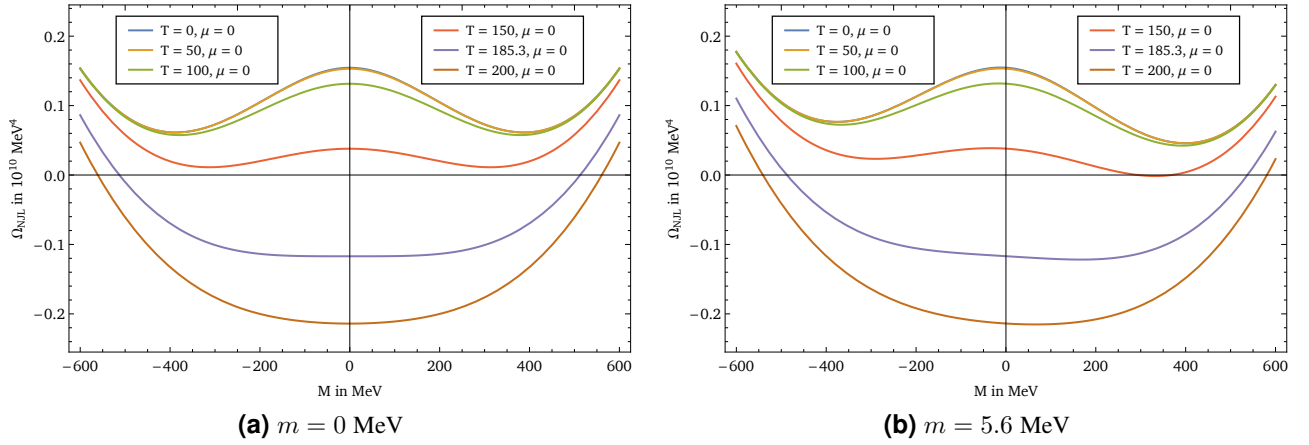


Figure 2.3: Thermodynamic potential as function of the constituent mass M for several temperatures T in MeV for zero chemical potential $\mu = 0$. The purple curve in the chiral limit case corresponds to the point at the second order phase boundary. The potential is shifted by a constant value of $\Omega_{off} = 1.97 \cdot 10^{10} \text{ MeV}^4$ such that the TCP has its global minimum with value zero.

In the left picture of figure 2.3 the different forms of the grand potential for points along the T -axis, that means $\mu = 0$, are shown. In the case of zero quark mass $m = 0$, the potential is symmetric around the trivial solution $M = 0$ of the gap equation which is due to the chiral symmetry. Starting with two local minima near $M = \pm 400 \text{ MeV}$ in the vacuum case, the central maximum decreases continuously while the two minima move towards each other for increasing temperatures. The two minima are at the same height for every temperature. Finally, at the second order phase boundary with $T = 185.3 \text{ MeV}$, the three stationary points merge and form a global minimum. This can be observed by the purple curve in the left figure. For temperatures in the restored phase, given by the brown curve, the global minimum decreases further. Hence, the stable constituent mass M changes continuously for zero chemical potential which accords to the definition of a second order phase transition.

Turning away from the chiral limit to the finite bare quark mass $m = 5.6 \text{ MeV}$ a different overall picture of the thermodynamic potential is shown in part (b) of figure 2.3. Here, $\Omega_{NJL}(M)$ keeps its general shape, however, the whole form is skewed to the right side. That means that chiral symmetry is explicit broken by

the finite quark mass since one cannot exchange M and $-M$. Moreover, the potential has higher values for negative masses with the main consequence that the trivial solution $M = 0$ from the chiral limit gets replaced by $M < 0$. Further, the skewed form leads to the existence of a global minimum for all temperatures along the axis. All in all, the general trend that there exist only three stationary points along the T -axis which merge all into the global minimum for high temperatures is similar. However, for nonzero current quark masses the well defined second order phase boundary of the chiral limit turns into a smooth crossover to the chirally restored region. At the crossover transition the mass varies smoothly from high to low values.

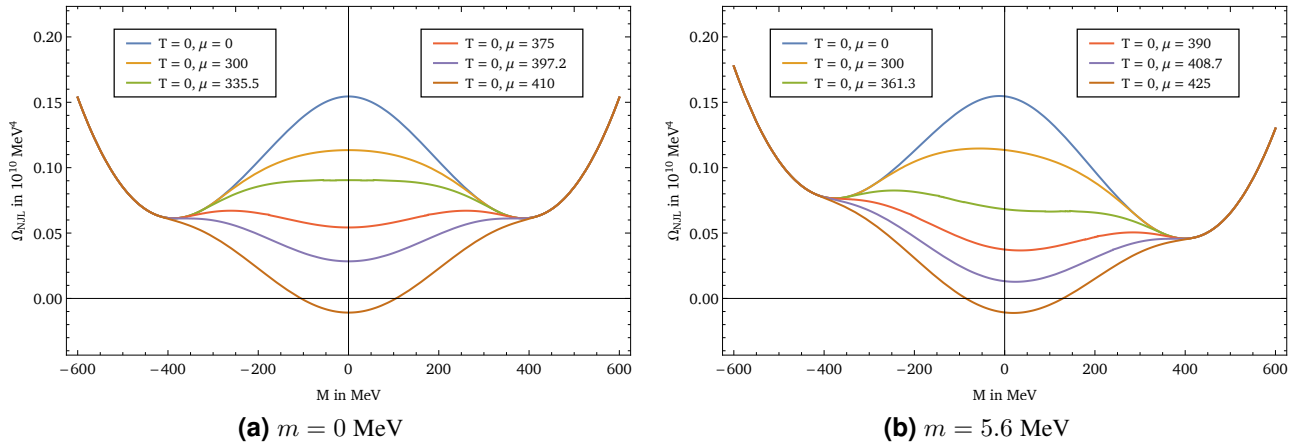


Figure 2.4: Thermodynamic potential as function of the constituent mass M for several chemical potentials μ in MeV in the zero temperature limit $T = 0$. The green and purple curves correspond to points on the left and right spinodal, respectively. The potential is shifted by a constant value of $\Omega_{off} = 1.97 \cdot 10^{10} \text{ MeV}^4$.

The graphics of figure 2.4 picture the different behavior of the potential in the special case of a zero temperature limit $T = 0$ for different chemical potentials. In particular, the position of the extrema gives rise to a comparison of the changing potential shapes which will be an important basis for the Ginzburg-Landau analysis in the next chapter. For this, it is useful to consider also the so-called spinodals in the following. In contrast to points along the T -axis, the thermodynamic potential for zero temperature changes in a way that for some points in the phase diagram five stationary points exist. For increasing chemical potentials, the central maximum decreases and forms a minimum in a way that besides two new maxima arise. The points in the phase diagram that correspond to the thermodynamic potential in a form where one of the outer minima just merge with an arised maxima to a saddle point determine the spinodals. Clearly, this can appear in two cases since the potential consists of a right and a left minimum. Thus, one can imagine two lines in the phase diagram, on both sides of the first order phase boundary, which form the spinodals and which will further intersect in the critical endpoint. A deeper discussion will follow in chapter 3. In the displayed figure, the green and purple lines correspond to the grand potential for vanishing temperatures at the left and right spinodal, respectively. While the situation in the chiral limit is again completely symmetric, the right figure gives a better view on the arising saddle points. Furthermore, the grand potential where the central minimum is at the same height as the right minimum corresponds to points directly on the first order phase boundary. In such a case, the potential

has five extrema and hence up to three possible solutions for the effective masses as values for the minima. This is especially visible in the red curves in figure 2.4 since these ones correspond to a point in the phase diagram between the spinodals which is not exactly located on the phase boundary. Since the central maximum turn to a minimum that decreases for increasing chemical potential, the global minimum is given first by the right minimum and after the first order boundary by the central minimum. Here, the stable constituent mass changes discontinuously due to the occurrence of the additional maxima along the μ -axis.

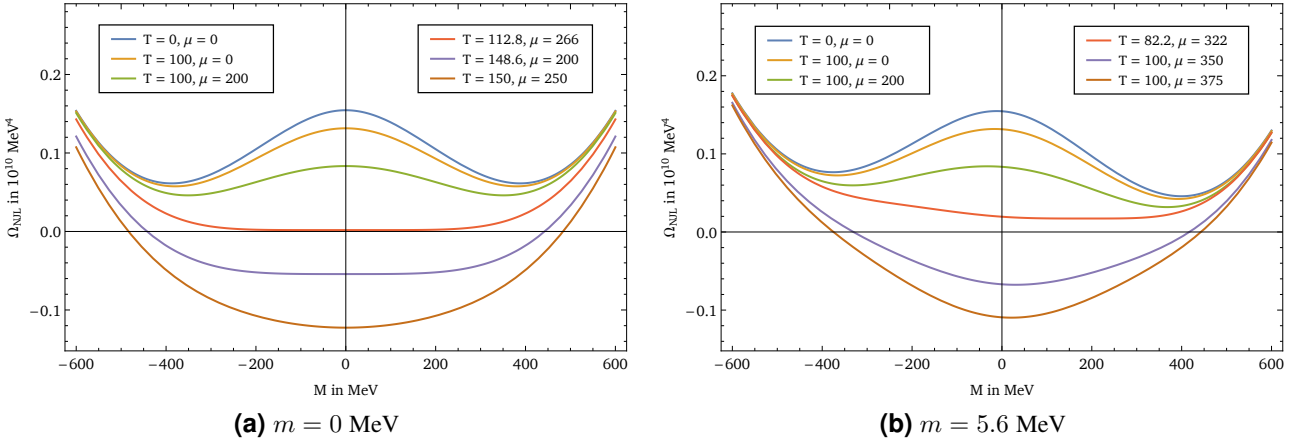


Figure 2.5: Thermodynamic potential as function of the constituent mass M at different points in the phase diagram with T and μ in MeV. The critical points are given by the red lines $T_c = 112.8$ MeV and $\mu_c = 266$ MeV in the chiral limit and $T_c = 82.2$ MeV and $\mu_c = 322$ MeV for $m = 5.6$ MeV. The potential is shifted by a constant value of $\Omega_{off} = 1.97 \cdot 10^{10}$ MeV⁴.

Finally, the figure 2.5 shows the behavior of the thermodynamic potential $\Omega_{NJL}(M)$ for different points in the phase diagram. In particular, the red curves show the flat shape of the potential for the critical points. These are given for the temperature and chemical potential combination where all five stationary points merge into one global minimum. Moreover, the spinodals meet at the critical points.

2.5 Solutions of the gap equation for zero chemical potential and zero temperature

After the previous discussion of the thermodynamic potential 2.28 the obtained results so far can be put into relation to a first analysis of the possible masses M . Therefore, this section provides the solutions of the derived gap equation 2.11 in the special cases of zero chemical potential and zero temperature limit, respectively. In the course of the subsequent introduction to Ginzburg-Landau analysis in chapter 3, the mass function will be considered also for nonzero combinations of temperature and chemical potential. Here, the solutions of the gap equation were determined numerically by searching the roots of

$$\frac{\partial \Omega_{NJL}(T, \mu; M)}{\partial M} \stackrel{!}{=} 0 \quad (2.30)$$

which states an equivalent formulation of the problem. This equation can be solved with an algorithm using the Newton methods for a defined starting point and a variant of the secant method for predefined solution intervals.

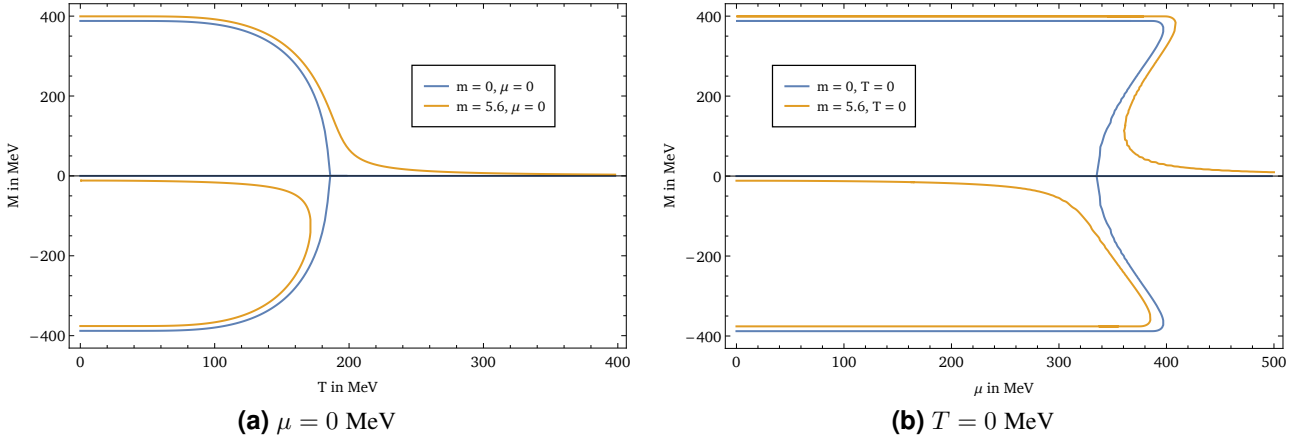


Figure 2.6: Comparison of the constituent mass M as function of the temperature T for $\mu = 0$ and as function of the chemical potential in the limit $T = 0$ for zero and nonzero quark mass m in MeV.

In figure 2.6 the results of the numerical calculations for the gap equation are depicted. The left picture shows the situation for zero chemical potential where in the case of the chiral limit symmetric solutions for the constituent mass in addition to the trivial solution $M = 0$ exist. These solutions correspond to the minima closely around $M = \pm 400$ visible in the course of the grand potential in figure 2.4. From that point onwards, the absolute values of the masses falls off and tend to zero for increasing temperatures where they finally reach the trivial solution as global minimum of the grand potential at the second order phase transition along the T -axis. This is called a second order phase transition since the function M is continuous but discontinuous in its derivative with respect to T . After the transition, only the zero solution exists corresponding to the area of restored chiral symmetry in the phase diagram. Due to the chiral symmetry the behavior of the effective masses is completely symmetric. For that reason, the case of finite bare mass does not have this symmetry. One can see negative solutions of the gap equation between the negative and trivial solution of the chiral limit. These solutions correspond to the two extrema of the grand potential in the negative half of figure 2.4 which are a result of the skewed course. For higher temperatures these solutions combine which gives the closed form when the left minimum merges the central maximum of the grand potential. The positive solution of the gap equation in this case starts right next to the chiral limit solution and falls off similar approaching the finite bare mass m asymptotically. This can be observed through the integral 2.20 in the gap equation 2.11 where the factor $(1 - n_k - \bar{n}_k)$ goes to zero for the limit of large temperatures. Moreover, this corresponds to the transition from the phase with broken chiral symmetry into the phase with approximately restored chiral symmetry. Since the constituent mass M is a continuous and smooth differentiable function of T , this is the crossover transition.

The right diagram of the figure shows the behavior of the constituent mass in the zero temperature limit. Actually, for the numerical calculations of the occurring integrals and equations the small finite value $T = 0.75$ MeV is used but indicated in the plots as zero. Otherwise, there would be many small fluctuations as solutions by using Newton methods which yield in turn to more small humps on the curves. Starting

with the blue curve for the chiral limit, the symmetric course of the solutions can be observed directly. Beginning at chemical potential of approximately $\mu = 335.5$ MeV there are up to five solutions of the gap equation. This fact corresponds to the observation that the thermodynamic potential has five extrema within the region of the spinodals. Furthermore, points on the spinodals can be obtained straightforwardly since there one has a saddle point instead of two extrema which means at least one solution less. In the graphic, the left spinodal is at $\mu = 335.5$ MeV where exactly three solutions for the effective mass exist, instead of five possible values when going to higher potentials. The right spinodal for zero temperature is close to $\mu = 397$ MeV because again the phenomenon occurs that only three solutions exist. Going to lower potentials, the saddle points become extrema such that one gets five masses. The results are the same as in the discussion of the spinodals through the grand potential in figure 2.4 and thus consistent.

In case of quark mass $m = 5.6$ MeV there are similar changes as in the case of zero chemical potential in the left figure. Here, the trivial solution $M = 0$ of the chiral limit moves into the negative area due to the skewed grand potential. For the positive solution the behavior for small chemical potentials is nearly the same as in the chiral limit. The positive effective masses are a little bit higher in the left picture since they are shifted by the bare mass. Again, the spinodals with saddle points of the grand potential in the second diagram of figure 2.4 can be obtained as the values of the chemical potential where just one positive constituent mass exists near to the area of three possible solutions. This is at the tips or humps of the curve which gives $\mu = 361.3$ MeV for the left and $\mu = 408.7$ MeV for the right spinodal at $T = 0$.

3 Ginzburg-Landau analysis

The Ginzburg-Landau (GL) theory is a mathematical physical continuum description of phase transitions, named after V. Ginzburg and L. Landau. Originally, it was used for describing superconductivity through macroscopic properties of the superconductor by applying general thermodynamic theorems. The main idea was the expansion of the free energy F in terms of an order parameter field that is nonzero below the focused phase transition [12]. Now, this basic idea will be applied in the situation of the phase transitions within the considered NJL model. For this, the chiral limit and finite bare mass cases were distinguished and for both of them a GL analysis will be developed. Moreover, this chapter will focus on the exact phase diagrams together with the position of the critical points which can be calculated by the analyzed GL coefficients of the expansion concept. The word 'exact' in this context has to be seen in relation to the used NJL model and not as exact in the sense of QCD since the NJL model is only an effective theory approach for that.

3.1 The Ginzburg-Landau theory

For the critical behavior of thermodynamical observables near phase transitions it is often not necessary to know all microscopic details or the exact form of the interaction. Therefore, it can be thought of a macroscopic continuum description for the phase transitions. To obtain this, one starts with the Landau theory which expands the free energy $F = -T \ln(\mathcal{Z})$ as a polynomial function of an order parameter ϕ near the phase boundary [13]. The order parameter ϕ is an appropriate macroscopic quantity which changes during the transition at the phase boundary in a characteristic way. Moreover, it describes the favored state for a given temperature. This quantity could be the magnetization for a ferromagnetic transition or the volume for the condensation of a gas but the choice of this quantity is in general not unique. The order parameter describes the changes at the phase transition such that it holds

$$\bar{\phi} = \begin{cases} 0 & T \geq T_c \\ \neq 0 & T < T_c \end{cases} \quad (3.1)$$

where $\bar{\phi}$ is the mean value of the order parameter. Since $\bar{\phi}$ is continuous at the boundary for $T = T_c$ it is possible to expand the free energy F in a neighborhood of the critical temperature T_c in powers of ϕ . The Ginzburg-Landau theory is a meaningful generalization of the Landau theory which leads to the Ginzburg-Landau ansatz by allowing a spatial dependence of the order parameter $\phi = \phi(\vec{x})$. The main idea is to include also spatial fluctuations of the order parameter because the crucial fluctuations for the physical system become more and more long-waved near the critical point such that the corresponding correlation length ξ diverges. Therefore, the Ginzburg-Landau model is justified especially near the critical point. The free energy in the GL theory is a functional $\mathcal{F}[\phi(\vec{x})]$ of the order parameter field. Hence, the minimum of the functional is searched with respect to all functions $\phi(\vec{x})$ that yields the necessary condition $\delta\mathcal{F} = 0$. Moreover, it is possible to find

an expression for the partition function \mathcal{Z} of the physical system [14]. The representation is given by a path integral over all possible configurations $\mathcal{D}\phi(\vec{x})$ of the order parameter and has the form:

$$\mathcal{Z} = \int \mathcal{D}\phi(\vec{x}) e^{-\beta\mathcal{F}[\phi(\vec{x})]} \quad (3.2)$$

According to statistical physics, the free energy can be written as a volume integral of the free energy density that is given by the value of the thermodynamic potential Ω . Turning now back to the aim of analyzing phase diagrams within the two-flavor NJL model, the grand potential can be seen as a functional of the effective mass. In the sense of Ginzburg-Landau, the effective mass is the order parameter field which depends in general on the spatial position, i.e. it holds $M = M(\vec{x})$. The central idea of the theory is to look at the expansion of the functional in terms of the order parameter and which results in the general expression

$$\Omega_{NJL}[M] = \Omega[M_0] + \frac{1}{V} \int d^3x \left(\alpha_1 \delta M(\vec{x}) + \dots + \alpha_{4,a} \delta M^4(\vec{x}) + \alpha_{4,b} (\nabla \delta M(\vec{x}))^2 + \dots \right) \quad (3.3)$$

if a combined gradient expansion is considered [15]. There, the gradients were treated in the same order as the magnitude of the order parameter. Further, the coefficients are functions of T and μ and the constituent mass was written as $M(\vec{x}) = M_0 + \delta M(\vec{x})$ for a constant part M_0 and a small varying $\delta M(\vec{x})$.

For the remaining course of the work, the expansion gets simplified since the main interest lies in constituent masses that don't depend on the spatial position since this would correspond to the analysis of inhomogeneous phases. Thus, the integral cancel against the volume and only a sum of terms without position dependence as well as without gradient terms remains. Then, the expansion takes the form

$$\Omega_{NJL}[M] = \sum_{n \in \mathbb{N}_0} \alpha_n(T, \mu) \cdot (M - M_0)^n \quad (3.4)$$

where the Ginzburg-Landau coefficients α_n with T and μ dependence are obtained by the partial derivative of the grand potential with respect to the constituent mass:

$$\alpha_n(T, \mu) = \left. \frac{1}{n!} \frac{\partial^n \Omega_{NJL}(T, \mu; M)}{\partial M^n} \right|_{M=M_0} \quad (3.5)$$

The potential gets expanded around the fixed effective mass M_0 that should correspond to a stationary point in the following analysis. Therefore, M_0 can be obtained as solution of the gap equation. In the next step, the behavior of the GL coefficients around the phase boundary will be investigated for the two cases of chiral limit and finite bare mass. This will lead to mathematical conditions which allow for a numerical calculation of the exact position of the TCP and CEP.

3.2 Analysis in the chiral limit

In the chiral limit $m = 0$, the position of the TCP can be calculated a little bit more easily as in the case of a nonzero current quark mass. This is due to a simplified expression of the expansion 3.4 since the trivial solution $M_0 = 0$ can be chosen as evaluation point for the GL coefficients. Also, this can be seen directly in figure 2.6 where the trivial solution of the gap equation is displayed together with the symmetric course of

the positive and negative mass. For the reason of chiral symmetry, all odd GL coefficients vanish and only the even ones remain such that the expansion finally takes the form

$$\Omega_{NJL}(T, \mu; M) = \sum_{n \in \mathbb{N}_0} \alpha_{2n}(T, \mu) \cdot M^{2n} \quad (3.6)$$

in this section. Additionally, it is assumed that all corrections of higher orders than four are generally positive. A profound investigation of the coefficients α_2 and α_4 will lead to the needed condition for the TCP.

3.2.1 The Ginzburg-Landau coefficients

The first step of the analysis is the determination of the Ginzburg Landau coefficients up to order four according to the made assumption. For order zero it holds

$$\alpha_0(T, \mu) = -C \left[\frac{\Lambda^4}{4} + \int_0^\infty dk k^2 T \left[\ln \left(1 + \exp \left(-\frac{k-\mu}{T} \right) \right) + \ln \left(1 + \exp \left(-\frac{k+\mu}{T} \right) \right) \right] \right] \quad (3.7)$$

which is the same as $\Omega_{NJL}(T, \mu; M = 0)$ and acts as offset at $M = 0$ for fixed T and μ . Here, the constant $C \equiv 6/\pi^2$ was introduced as the pre-factor of the integral terms in the grand potential 2.28. Indeed, the coefficients α_2 and α_4 play the major role such that it is sufficient to focus on them. One yields the relation

$$\alpha_2(T, \mu) = \frac{1}{4G} - \frac{C}{2} \left[\frac{\Lambda^2}{2} - \int_0^\infty dk k \left(\frac{1}{1 + \exp \left(\frac{k-\mu}{T} \right)} + \frac{1}{1 + \exp \left(\frac{k+\mu}{T} \right)} \right) \right] \quad (3.8)$$

for the second coefficient which has also a pure analytical representation using the dilogarithm such that it holds:

$$\alpha_2(T, \mu) = \frac{1}{4G} + T^2 + \frac{3(2\mu^2 - \Lambda^2)}{2\pi^2} + \frac{3T^2}{\pi^2} \left[\text{Li}_2 \left(-e^{-\frac{\mu}{T}} \right) + \text{Li}_2 \left(-e^{\frac{\mu}{T}} \right) \right] \quad (3.9)$$

Nevertheless, it is used the integral expression for applying numerically methods in the same way as for α_4 that has the following form:

$$\alpha_4(T, \mu) = -\frac{C}{4!} \left[3 - \int_0^\Lambda dk \frac{3}{k} + \int_0^\infty dk \frac{3}{k} \left(\frac{1}{1 + \exp \left(\frac{k-\mu}{T} \right)} + \frac{1}{1 + \exp \left(\frac{k+\mu}{T} \right)} \right) \right] \quad (3.10)$$

Despite, the first integral in the relation for α_4 is infrared divergent, the integrals can be solved numerically since together with the second integral one has in total a convergent expression. In the improper integrals often terms like $\left(1 + \exp \left(\frac{k-\mu}{T} \right) \right)^{-1}$ appear. These correspond to the quark occupation numbers for zero constituent mass in the energy relation. Next, the qualitative behavior of the thermodynamic potential for different regions within the phase diagram will be considered. From that behavior, sign restrictions for the coefficients α_2 and α_4 can be derived by the presumption of only positive high order coefficients. The different occurring forms of the potential are displayed in figure 3.1. In the case where all coefficients are positive, the restored phase with global minimum $M = 0$ is obtained. For the combinations of μ and T where α_4 is positive and it holds $\alpha_2 < 0$, nontrivial solutions $M \neq 0$ are favored. This gives just the broken phase with the two minima on the same height and a central maximum. For vanishing α_2 the solutions $M = 0$ are favored again and yield

the second order phase transition. Going on to cases of negative GL coefficients α_4 , the first order phase transition becomes possible for $\alpha_2 > 0$ with a grand potential form containing five stationary points. At the TCP the first order phase boundary meets the second order phase boundary which results in the distinct condition $\alpha_2 = \alpha_4 = 0$.

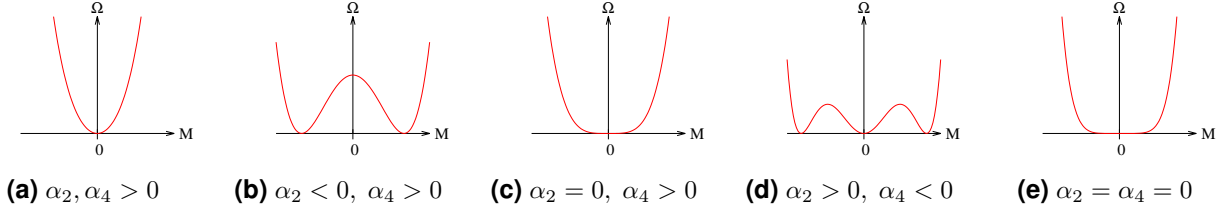


Figure 3.1: Different qualitative forms of the grand potential Ω_{NJL} as function of the constituent mass order parameter M in the chiral limit, taken from [16]. The behavior corresponds to (a) restored phase, (b) broken phase, (c) second order phase transition, (d) first order phase transition and (e) TCP.

Altogether, the analysis of the different characteristic shapes of the grand potential as function of the constituent mass leads to the condition

$$\text{TCP: } \alpha_2(T, \mu) = \alpha_4(T, \mu) = 0 \quad (3.11)$$

for the tricritical point. This allows a numerical calculation of the exact position of the TCP such that the next part will deal with the exact phase diagram in the chiral limit.

3.2.2 Phase diagram with TCP

The results of the previous analysis can be evaluated now using concrete values for the parameters given by the set 2.29 as well as an adaptive algorithm for the numerical computation of the occurring integrals. The searched roots of the Ginzburg-Landau coefficient functions can be calculated by using Newton and secant methods again. The left graphic in figure 3.2 shows the course of the solutions for $\alpha_2(T, \mu) = 0$ and $\alpha_4(T, \mu) = 0$ which intersect in the TCP since this is exactly the statement of the condition 3.11. Therefore, the TCP can be calculated exactly within numerical uncertainties and under the assumption of positive higher order GL coefficients. The TCP values are $T_c = 112.78$ MeV for the critical temperature as well as $\mu_c = 266.04$ MeV as critical chemical potential. The part of $\alpha_2 = 0$ on the left side of the TCP corresponds to the second order phase transition as discussed before in figure 3.1. Moreover, the solutions below the TCP yield the left spinodal since there is exactly a saddle point given by $\alpha_2 = 0$ as the left minimum just merges the central maximum of the grand potential. The right spinodal can be calculated in the same way, however, it is necessary to use a different evaluation point M_0 in the relation 3.5. Therefore, one obtains the right spinodal by solving the equations

$$\alpha_1(T, \mu; M_0 \neq 0) = \alpha_2(T, \mu; M_0 \neq 0) = 0 \quad (3.12)$$

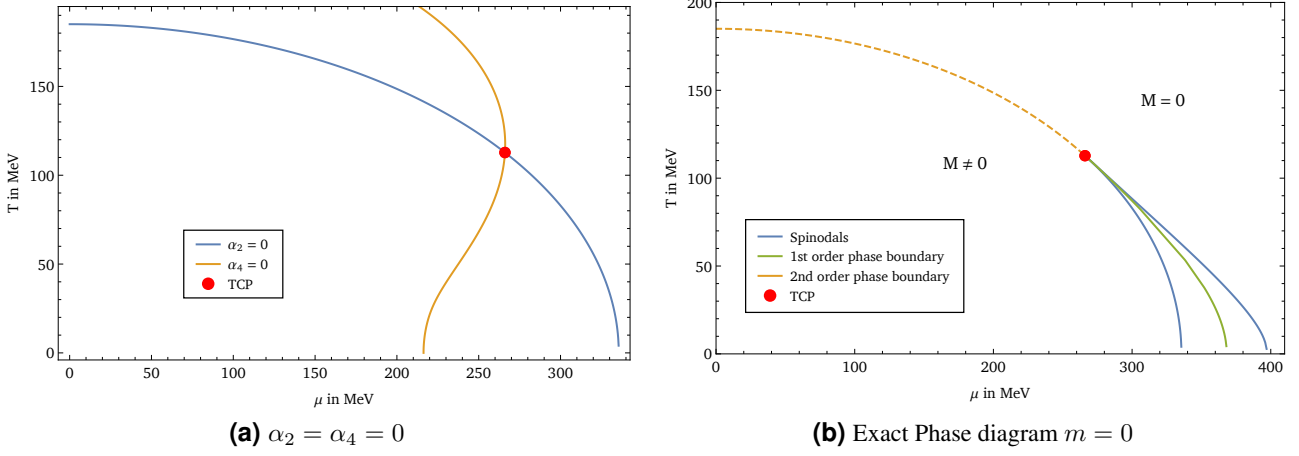


Figure 3.2: Chiral limit phase diagram with TCP as intersection of the GL coefficients and second order phase boundary by the $\alpha_2=0$ curve.

for constituent masses $M_0 \neq 0$. That means, one has to search all the $\alpha_2 = 0$ curves in the phase diagram. Here, α_1 can be nonzero since a different mass for evaluation is used. The statement $\alpha_1(T, \mu) = 0$ is therefore in general equivalent to the gap equation 2.11. The effective masses M on the right spinodal turn thus from high values around $M = 400$ MeV to zero at the TCP where both spinodals intersect. At this point also the first order phase boundary joins which corresponds to such points in the phase diagram where both minima of the grand potential within the spinodal region are at equal height. Hence, the boundary can be calculated with a solution M_0 of the gap equation, given by $\alpha_1 = 0$, which also solves the equation

$$\Omega_{NJL}(T, \mu; M_0) - \Omega_{NJL}(T, \mu; M = 0) = 0 \quad (3.13)$$

which means that both minima lead to the same value of the potential. The obtained tuples (T, μ) represent the first order phase boundary displayed as green curve in the right picture of figure 3.2. Next, the expression for the GL coefficient α_1 will be investigated directly and the possible constituent masses in the chiral limit can be analyzed for points away from the vacuum.

3.2.3 Constituent mass functions

Often, it can be useful to take a closer look on the exact behavior of the gap equation solutions. That means the constituent masses can be seen as functions over the chemical potential if temperature is fixed. From the shape of the resulting mass functions the TCP and also the spinodals can be identified directly. For that purpose, a concrete expression for the general α_1 without evaluation point is needed. The calculation of the first derivative is straightforward and yields

$$\alpha_1(T, \mu; M) = \frac{\partial \Omega_{NJL}}{\partial M} = \frac{M}{2G} - C \left[\int_0^\Lambda dk \frac{k^2 M}{E_{\vec{k}}} - \int_0^\infty dk \frac{k^2 M}{E_{\vec{k}}} (n_k + \bar{n}_k) \right] \quad (3.14)$$

which is equivalent to the gap equation 2.11 in the case of $\alpha_1(T, \mu; M) = 0$. Solutions of this equation were

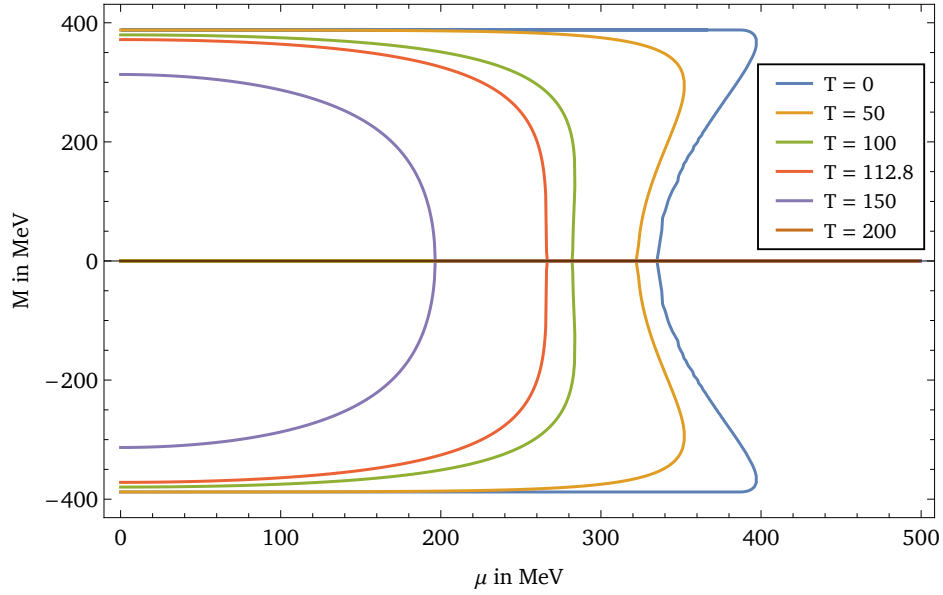


Figure 3.3: Constituent mass as function of the chemical potential in the chiral limit for different fixed temperatures.

already discussed in the cases $T = 0$ and $\mu = 0$ in section 2.5. Now, also different fixed temperatures were taken to investigate changes of the shape of the mass function. The results are displayed in figure 3.3. The general shape for temperatures below the TCP is the same but turn more and more to lower chemical potentials. Simultaneously, the number of possible solutions shrink from up to five back to three above the TCP. Moreover, the solutions for zero chemical potentials become lower, since the two minima of the grand potential move to the center for a global minimum. For the case with $T = 200$ MeV only the trivial solution $M = 0$ remains. The tips of the curves for low temperatures indicate the points where a saddle point arises and therefore they correspond to the spinodals. These peaks disappear continuously and for the curve at the critical temperature $T_c = 112.8$ MeV only a vertical line at the front, intersecting the μ -axis at the critical chemical potential $\mu_c = 266$ MeV, remains. For higher temperatures, the shape continues to an increasingly round form at the right front. Thus, an accurate analysis of the mass functions already enables to find the critical area and therefore the temperature and potential at the TCP.

3.3 Analysis for nonzero quark mass

For finite bare masses $m \neq 0$ away from the chiral limit, the situation is more complicated since there is no exactly restored phase. The zero solution is not a solution of the gap equation in this case and therefore, the grand potential should be expanded around another stationary point of the potential. That means first a solution M_0 of $\alpha_1(T, \mu; M_0) = 0$ is needed for the constituent mass which will be used as evaluation point for the coefficients in relation 3.5. Further, all Ginzburg-Landau coefficients remain in the expansion since the argument of symmetric solutions due to chiral symmetry does not hold anymore as one can see directly in figure 2.5. It will be seen that again a suitable condition for the critical endpoint can be derived applying a deeper analysis of the Ginzburg-Landau coefficients α_1 , α_2 and α_3 .

3.3.1 The Ginzburg-Landau coefficients

Now, it is necessary to investigate the qualitative behavior of the first three GL coefficients to determine a condition for the exact position of the CEP. For the sake of clarity, the individual expressions for the α_n are not stated explicitly since the occurring derivatives lead to many terms. Instead, the resulting forms of the grand potential as function of the constituent mass in different areas of the phase diagram are displayed in figure 3.4. From this, one can again derive the varying sign restrictions for the Ginzburg-Landau coefficients. The constituent mass M_0 denotes therefore a stationary point of the grand potential such that the first GL coefficient α_1 vanishes and a function $M_0(T, \mu)$ can be derived from $\alpha_1(T, \mu; M_0) = 0$.

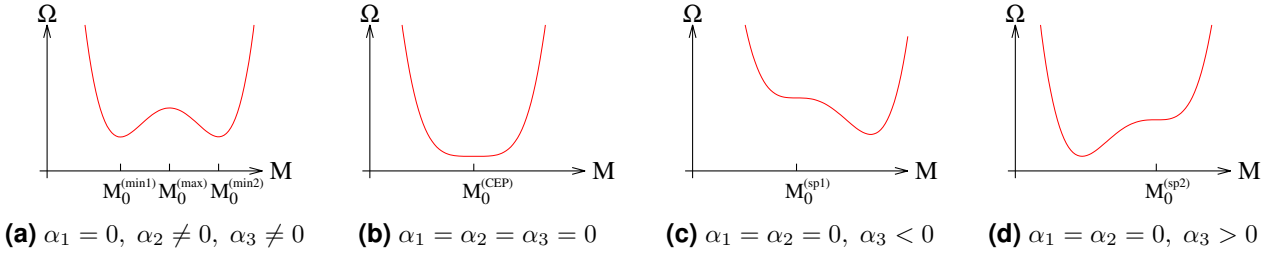


Figure 3.4: Different qualitative forms of the grand potential Ω_{NJL} as function of the constituent mass order parameter M for finite bare mass, taken from [16]. The behavior corresponds to (a) first order phase boundary, (b) CEP, (c) left spinodal and (d) right spinodal.

In the first picture, the first order phase boundary yields a grand potential with two degenerate minima beside a central maximum. Moving along this boundary to the critical endpoint, the three stationary points merge into one global minimum such that there the additional condition $\alpha_2 = 0$ holds. Another way to reach the CEP is by going along the spinodals. Since there one has a saddle point, the conditions $\alpha_2 = 0$ and $\alpha_3 < 0$ for the left and $\alpha_3 > 0$ for the right spinodal hold, respectively. The two spinodals meet at the CEP such that at this point $\alpha_3 = 0$ is also a necessary requirement. In summary, the searched condition for the critical endpoint is given by

$$\text{CEP: } \alpha_1(T, \mu; M_0) = \alpha_2(T, \mu; M_0) = \alpha_3(T, \mu; M_0) = 0 \quad (3.15)$$

in the case of finite quark masses for an Ginzburg-Landau expansion around a stationary point M_0 of the grand potential. Now, one can again turn to the exact phase diagram for which the CEP can be calculated numerically with the obtained condition.

3.3.2 Phase diagram with CEP

Applying the same numerical methods as in the chiral limit case together with the parameter set 2.29 for the previously derived condition 3.15 allows a nearly exact computation of the critical endpoint. The solution of the system of equations is a temperature of $T_c = 82.19$ MeV and a chemical potential of $\mu_c = 322.02$ MeV. For the constituent mass at the CEP one obtains $M_0 = 186.61$ MeV. The phase diagram can be calculated also in this case from the GL coefficients as functions of T and μ . Since there is always a solution of the gap

equation $\alpha_1 = 0$ for the expansion needed, one can think about using the negative masses M_0 as well. For that reason, the left graphic in figure 3.5 shows also solutions of setting $\alpha_2(T, \mu; M_0)$ and $\alpha_3(T, \mu; M_0)$ to zero for an expansion with negative mass M_0 indicated by dotted lines. Though, the qualitative shape of the $\alpha_2 = 0$ and $\alpha_3 = 0$ curves for negative constituent masses does not show anything revealing for the underlying phase diagram. Especially, the two curves do not intersect. However, the CEP turns out as expected as intersection of the $\alpha_3 = 0$ curve with the spinodals which correspond to the $\alpha_2 = 0$ curves for positive masses M_0 obtained by solving the equations 3.12.

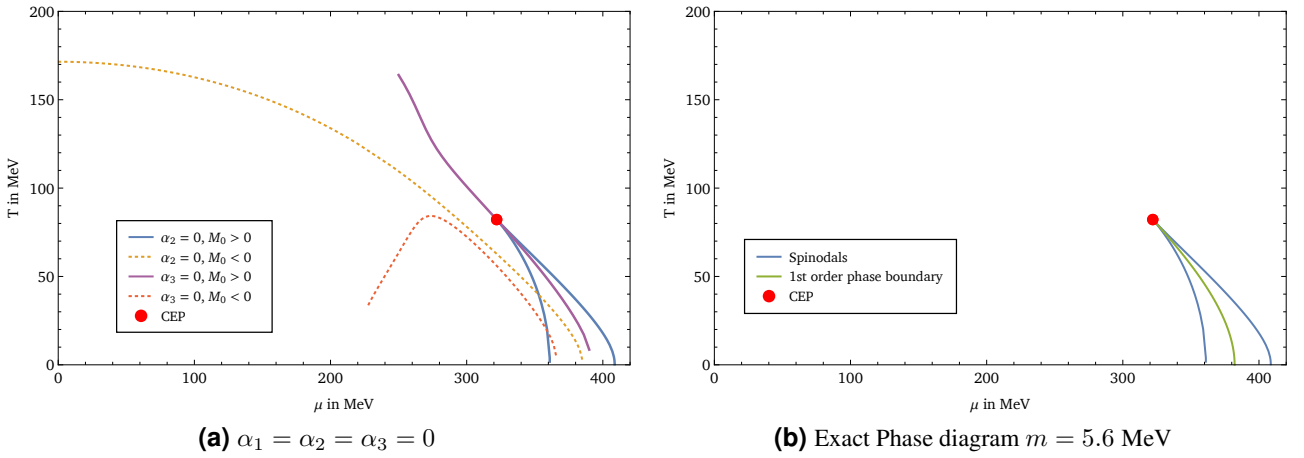


Figure 3.5: Finite bare mass phase diagram with CEP as intersection of the spinodals as well as the GL coefficients set to zero and evaluated for positive and negative solutions of the gap equation.

The right picture in figure 3.5 shows the pure phase diagram with the two spinodals as well as the first order phase boundary. The latter one is calculated again by searching for points in the phase diagram where the right and central minimum of the grand potential $\Omega_{NJL}(T, \mu; M_0)$ are at equal height. Above the CEP, a smooth crossover between the chirally broken and restored phase follows instead of the second order phase transition in the chiral limit. This crossover is, however, not depicted explicitly.

3.3.3 Constituent mass functions

Finally, it is again useful to consider the solutions of the gap equation as functions of the chemical potential for different fixed temperatures. The first Ginzburg-Landau coefficient defines the gap equation and gets one additional term due to the nonzero quark mass which states:

$$\alpha_1(T, \mu; M) = \frac{\partial \Omega_{NJL}}{\partial M} = \frac{M - m}{2G} - C \left[\int_0^\Lambda dk \frac{k^2 M}{E_{\vec{k}}} - \int_0^\infty dk \frac{k^2 M}{E_{\vec{k}}} (n_k + \bar{n}_k) \right] \quad (3.16)$$

The resulting solutions for the constituent mass are shown in figure 3.6. In comparison to figure 3.3 the solutions are not symmetric anymore and the positive solutions move asymptotically down and would approach the current quark mass for high chemical potentials if the second integral in equation 3.16 had the same cut-off.

The solution curves in the negative half are closed and correspond to the central and left stationary point of the grand potential that is skewed for nonzero quark masses.

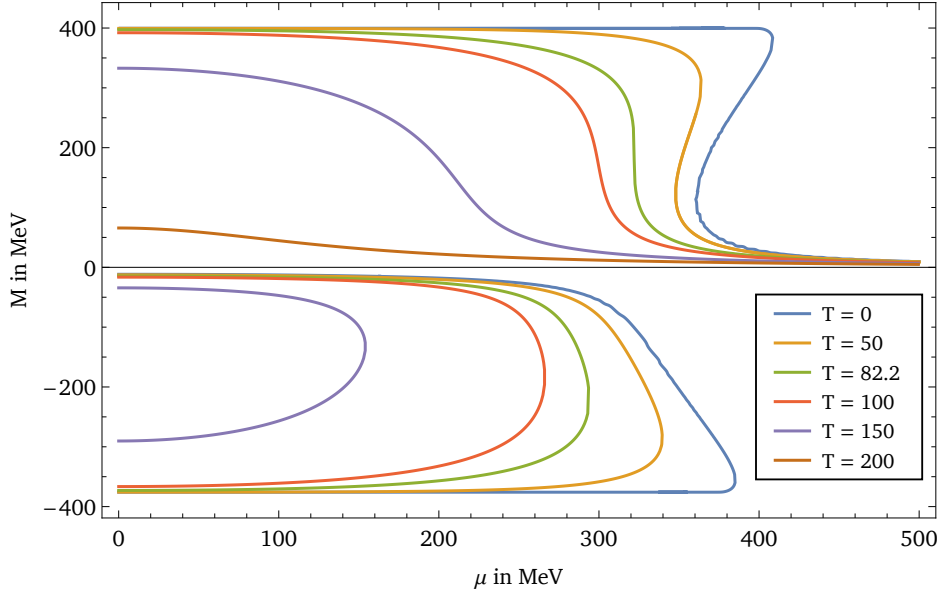


Figure 3.6: Constituent mass as function of the chemical potential for quark mass $m = 5.6$ MeV with different fixed temperatures.

In the area of high chemical potentials the figure allows the approximately determination of the spinodals and the critical endpoint by the change in the number of possible constituent mass solutions. Therefore, one has to consider the curves in the positive half for chemical potentials in the area of three solutions. Going to lower and higher potentials yield a point at the tip where exactly two positive solutions remain. Moving further, only one positive mass is possible. At this tip point, two stationary points of the grand potential merge and the saddle point at the corresponding spinodal remains. The critical endpoint, according to the green curve, is given for the solution where the two tips are at equal chemical potential, merging in one point with vertical line. Turning to higher temperatures than $T_c = 82.19$ MeV leads to curves where for every chemical potential only one positive solution is possible. For very high temperatures, for instance $T = 200$ MeV, there exists no negative constituent mass as solution.

4 Taylor series approximation of TCP and CEP

In the previous chapter, it was shown that the Ginzburg-Landau analysis enables the numerical calculation of the exact position of the TCP and CEP in the NJL model in mean-field approximation. Therefore, two criteria for the Ginzburg-Landau coefficients at the critical points were derived in 3.11 and 3.15 by an analysis of the sign restriction for different points in the phase diagram. However, the main purpose of this work is to check how good an approximation of the critical points can be within using the GL coefficients as underlying quantity. Often an exact calculation is not possible, for example in the lattice QCD where one can work only with zero chemical potential. Nevertheless, information for finite μ can be obtained by a classical Taylor series expansion around $\mu = 0$ which are practicable around up to order eight [17]. This was also done as attempt to approximately identify the critical endpoint by a Taylor series of the pressure p in [18]. The main idea results from the fact that the pressure p is a quantity which can be handled also in lattice QCD by an expansion. Unfortunately, the results in [18] show that the approximation is nearly exact for a range of up to $\mu = 100$ MeV and then the solution goes away from the second order phase boundary, such that an approximation of the CEP is not possible. Now, the Ginzburg-Landau coefficients represent a new kind of physical quantity which can be used for an Taylor series expansion. In the Nambu-Jona-Lasinio model where the exact phase diagram is calculated for comparison, the Ginzburg-Landau coefficients will be expanded next in Taylor series expansions of the form

$$\alpha_n(T, \mu) = \sum_k c_{n,k}(T) \cdot \mu^k \quad (4.1)$$

where for the k -th Taylor coefficient $c_{n,k}$ of the n -th GL coefficient it holds:

$$c_{n,k}(T) = \left. \frac{1}{k!} \frac{\partial^k \alpha_n(T, \mu)}{\partial \mu^k} \right|_{\mu=0} \quad (4.2)$$

In the following sections, the TCP and CEP will be calculated for different orders of the Taylor polynomial by using the conditions of the Ginzburg-Landau analysis and finally the approximated values will be compared to the exact results. This will show, how good such an Ginzburg-Landau and Taylor series attempt for approximations of critical points in future calculations will be. For the reason of the trivial solution $M = 0$ as evaluation point in the chiral limit, it can be already imagined that the Taylor coefficients for $m = 0$ are slightly easier to calculate and that the computations are noticeably faster. This will result in a somewhat better approximation of the TCP than the CEP by the Taylor approach.

4.1 Approximation of the TCP

For an approximation of the tricritical point a Taylor series for both, the GL coefficient α_2 and α_4 , in the chiral limit $m = 0$ with constituent mass $M = 0$ is needed. First, the coefficient $\alpha_2(T, \mu)$ is considered with an

approximation by the Taylor polynomial $P_{n,k}(T, \mu)$ of order $k = 2$. Taylor polynomials of odd order do not improve the approximation since these coefficients vanish due to the chemical potential Ω_{NJL} which is an even function in μ . The figure 4.1 shows in the first picture the approximation of the $\alpha_2 = 0$ curve through the solutions of $P_{2,2} = 0$. As one can see, the approximation of the Taylor polynomial of second order $P_{2,2} = 0$ already gives a perfect solution for the $\alpha_2 = 0$ curve. Therefore, one can expand this GL coefficient 3.9 into the Taylor polynomial that is given by the expression:

$$P_{2,2}(T, \mu) = \frac{1}{4G} - \frac{3\Lambda^2}{2\pi^2} + \frac{T^2}{2} + \frac{3\mu^2}{2\pi^2} \quad (4.3)$$

This result will be used for the following calculations of the TCP approach. In the next step, the α_4 coefficient will be expanded into Taylor series up to order 34. Again, the odd Taylor coefficients vanish due to the argument of the even function $\Omega_{NJL}(\mu) = \Omega_{NJL}(-\mu)$.

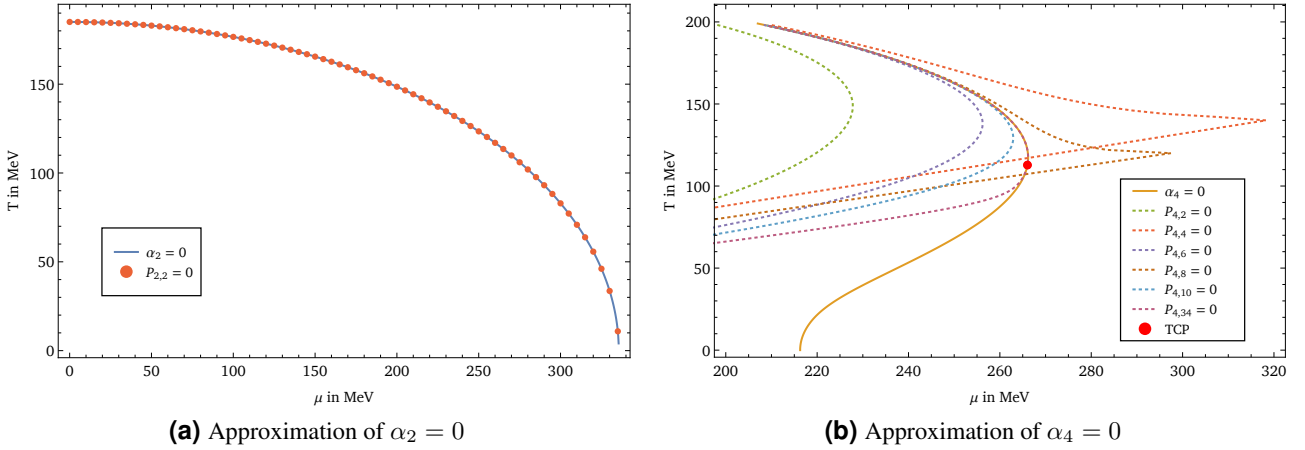


Figure 4.1: Taylor series approximation of the GL coefficients $\alpha_2 = 0$ and $\alpha_4 = 0$ for different orders k of $P_{n,k}$.

The right picture of figure 4.1 shows clearly how higher orders of the Taylor expansion come closer to the originally $\alpha_4 = 0$ curve. For the polynomial of order 34, the TCP is nearly exactly approximated, however, the shape of the curves have no accordance for low temperatures, going apart at around $T = 90$ MeV. Nevertheless, the Taylor polynomial approach is satisfactory and already in the same magnitude for the lower orders. The polynomial of order ten has its tip at a chemical potential of $\mu = 262.9$ MeV which is close to μ_c . Moreover, it can be seen in the picture, that the Taylor polynomials of order $k \equiv 0 \pmod{4}$ leads to curves with different shape which approximate the overall $\alpha_4 = 0$ curve from the right side instead of the better curve approximation from the left side for orders $k \equiv 2 \pmod{4}$. Despite this, the approximation of the TCP is also very good for these polynomials such that the intersection with the second Ginzburg-Landau coefficient will be calculated for all of the depicted Taylor polynomials. The corresponding Taylor coefficients for the expansion of α_4 in equation 3.10 can be expressed by integrals over hyperbolic functions in the following way:

$$c_{4,0}(T) = -\frac{C}{24} \left[3 - \int_0^\Lambda dk \frac{3 \tanh\left(\frac{k}{2T}\right)}{k} + \int_\Lambda^\infty dk \frac{6}{k + ke^{\frac{k}{T}}} \right] \quad (4.4)$$

$$c_{4,2}(T) = -\frac{C}{48} \left[\int_0^{\infty} dk \frac{12 \operatorname{csch}^3\left(\frac{k}{T}\right) \sinh^4\left(\frac{k}{2T}\right)}{kT^2} \right] \quad (4.5)$$

For the second one and for the fourth coefficient it holds

$$c_{4,4}(T) = -\frac{C}{576} \left[\int_0^{\infty} dk \frac{3 \left(\cosh\left(\frac{k}{T}\right) - 5 \right) \operatorname{sech}^4\left(\frac{k}{2T}\right) \tanh\left(\frac{k}{2T}\right)}{4kT^4} \right] \quad (4.6)$$

where $C = 6/\pi^2$ is again the integral pre-factor from the previous chapter. For the sake of clarity, only the first three coefficients up to order four are stated explicitly.

Table 4.1: Results for the Taylor series approximation of the TCP by $P_{2,2}(T, \mu) = P_{4,k}(T, \mu) = 0$ for different Taylor orders k of the fourth Ginzburg-Landau coefficient. The exact tricritical point is located at the values $\mu_c = 266.04$ MeV and $T_c = 112.78$ MeV in the phase diagram.

Order k	Approximated critical potential μ_c^k in MeV	Approximated critical temperature T_c^k in MeV
2	226.33	136.61
4	240.38	131.56
6	252.46	121.90
8	261.39	117.85
10	260.40	116.71
34	266.03	112.79

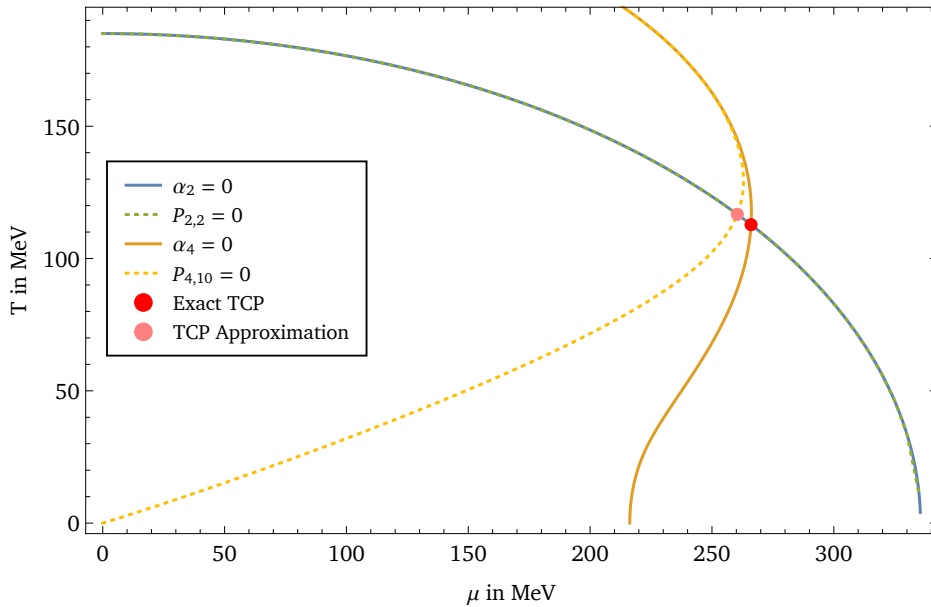


Figure 4.2: Exact and approximated TCP in the chiral limit given as solution of the systems $\alpha_2 = \alpha_4 = 0$ and $P_{2,2} = P_{4,10} = 0$, respectively.

In the next step, the intersections of the $P_{2,2} = 0$ curve with different curves by the Taylor polynomials $P_{4,k} = 0$ were calculated. Solving the system of equations with the mentioned numerical methods yields the approximated tricritical points which are listed in table 4.1. Comparison with the exact TCP values

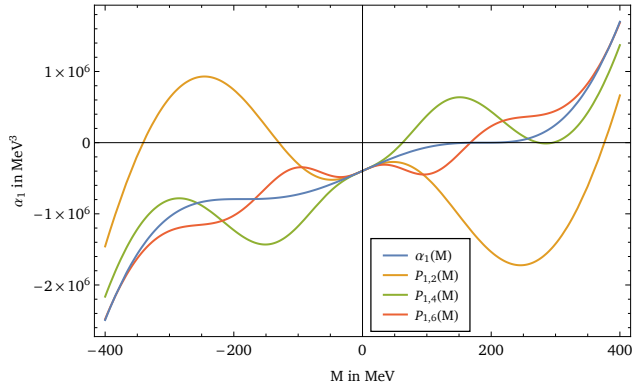
$T_c = 112.78$ MeV and $\mu_c = 266.04$ MeV from the Ginzburg-Landau analysis leads to the result that order $k = 34$ gives nearly the exact result. Nevertheless, the approximated values for low orders move quickly in the direction of the TCP such that order $k = 10$ and $k = 8$ yield also suitable results in the same magnitude of the exact TCP. Moreover, the low orders have an much easier analytic expression and can be calculated faster.

Finally, one can display the results of this section in figure 4.2 where the situation for the exact Ginzburg-Landau coefficient with TCP is compared to the approach by the Taylor polynomials of order two and ten together with the approximated TCP. The figure shows, that the Taylor series attempt yields at least a useful approximation of the tricritical point in the chiral limit and that one can work likely with the polynomial $P_{4,10}(T, \mu)$ for any approximation.

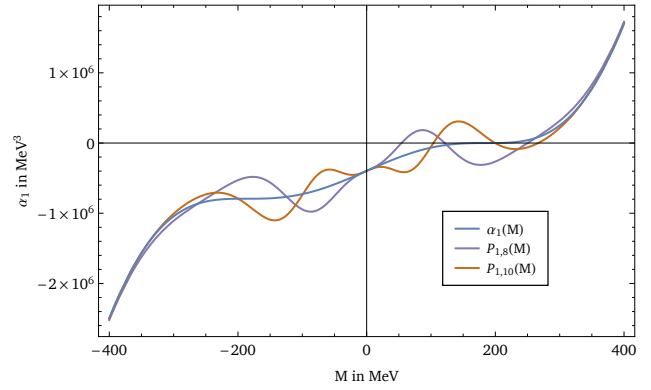
4.2 Approximation of the CEP

In this section, the more complicated case of a finite quark mass $m = 5.6$ from the parameter set 2.29 is considered. Therefore, the Taylor series expansion 4.1 is needed for the first three Ginzburg-Landau coefficients α_1 , α_2 and α_3 since they all contribute to the Ginzburg-Landau expansion of the grand potential in 3.4. The CEP can be calculated by the criterion 3.15 which is the origin of the difficulty in this case. First, one has to solve the gap equation $\alpha_1(T, \mu) = 0$ as Taylor polynomial approximation. That yields resulting constituent masses M'_0 which differ from the actual ones and the scale of the difference depends on the order of the series expansion. The constituent mass M'_0 is then needed as evaluation point for the second and third Ginzburg-Landau polynomial, such that the results of these GL coefficients in turn differ due to the shifts in the constituent mass solutions M_0 . Solving all three equations together leads to the critical endpoint, but the quality of the approximated solution for low orders will be not as good as in the chiral limit case.

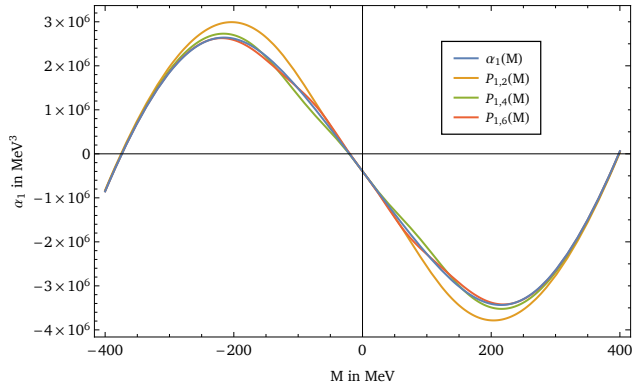
The Taylor coefficients for the finite quark mass case were not stated explicitly at this point, since these are lengthy expressions without further insides, already for low orders. For the derivative of the Ginzburg-Landau coefficients with respect to μ , only the second integral in the expression of the grand potential Ω_{NJL} in relation 2.28 has to be considered due to the occurrence of the chemical potential. Moreover, the expressions get quickly unwieldy and thus the computation for higher orders than $k = 8$ and $k = 10$ depending on the coefficient n is not possible or takes several hours. For this reason, the Taylor series expansion $P_{n,k}(T, \mu)$ is proceeded up to order $k_1 = 10$ for α_1 and up to order $k_2 = k_3 = 8$ for the coefficients α_2 and α_3 . The increasing quality of the Taylor approximation for the first GL coefficient is depicted in figure 4.3. There, one can see the approximation up to order $k_1 = 10$ of $\alpha_1(M)$ as function of the constituent mass M at the CEP. It is shown well, that the fluctuations in the depicted area get less for higher orders and the Taylor polynomial curves come closer to the shape of α_1 . For the Taylor expansion $P_{1,2}$ there are also negative masses as zeros of the function which are not present in the exact GL coefficient. For the highest order $k_1 = 10$, there are still three zeros but they are all located directly next to the unique zero of $\alpha_1(M)$. The situation for the chirally broken and restored phase in the pictures below is much better.



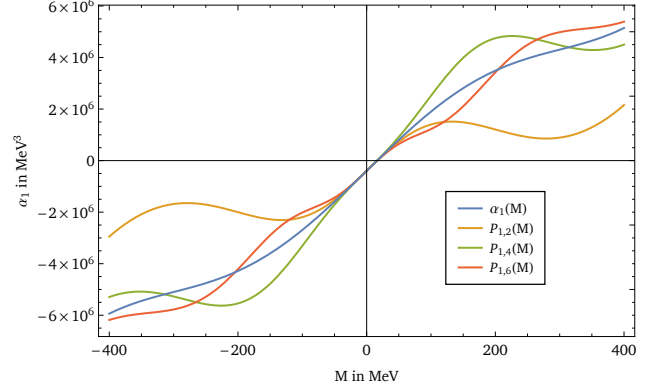
(a) $T_c = 82.19$ MeV and $\mu_c = 322.02$ MeV



(b) $T_c = 82.19$ MeV and $\mu_c = 322.02$ MeV

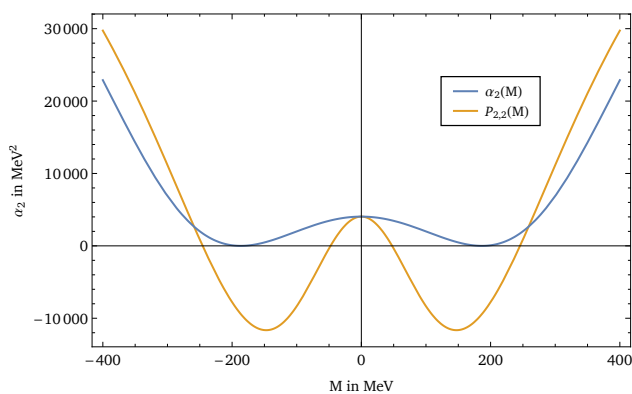


(c) $T = 50$ MeV and $\mu = 200$ MeV

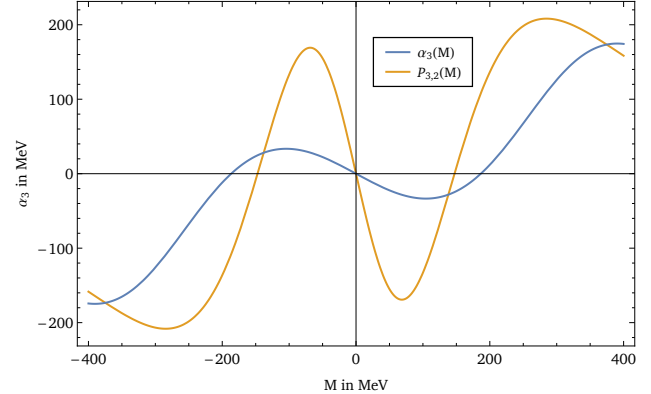


(d) $T = 100$ MeV and $\mu = 400$ MeV

Figure 4.3: Taylor polynomials $P_{1,k_1}(M)$ as functions of the constituent mass M for the Ginzburg-Landau coefficient α_1 at the CEP and for two other points in the phase diagram for different Taylor orders k_1 .



(a) Approximation of $\alpha_2 = 0$



(b) Approximation of $\alpha_3 = 0$

Figure 4.4: Second order Taylor series approximation of the Ginzburg-Landau coefficients α_2 and α_3 by $P_{n,2}(M)$ as functions of the constituent mass M at the critical endpoint $T_c = 82.19$ MeV and $\mu_c = 322.02$ MeV. Note: Higher orders of the Taylor series approximation were not shown due to the especially long computation time.

Next to the better overall approximation of the curves, the zero of $\alpha_1(M)$ is already approximated well for low orders. In figure 4.4, the situation at the CEP for the GL coefficients $\alpha_2(M)$ and $\alpha_3(M)$ as functions of the effective mass is displayed for an approximation of second order $P_{n,2}$. The computation for the higher order plots is aborted after a half day due to the long computation time already for order four. However, the approximation for the third coefficient reproduces already the overall shape and the vague position of the zeros. The Taylor series expansion of order two for the second GL coefficient has also the same shape but one gets four instead of two zeros for $\alpha_2(M) = 0$. Finally, it seems to make sense using a high Taylor order for the first GL coefficient since this yields the constituent mass solution and further to use order six or eight for the approximation of $\alpha_2(T, \mu)$ and $\alpha_3(T, \mu)$.

Table 4.2: Results for the Taylor series approximation of the CEP by $P_{1,k_1} = P_{2,k_2} = P_{3,k_3} = 0$ for different Taylor orders k_1, k_2 and k_3 of the first three Ginzburg-Landau coefficients. The exact critical endpoint is located at the values $\mu_c = 322.02$ MeV and $T_c = 82.19$ MeV in the phase diagram for a constituent mass of $M_0 = 186.61$ MeV.

Order k_1	Order k_2	Order k_3	Approx. μ'_c in MeV	Approx. T'_c in MeV	Approx. M'_0 in MeV
2	2	2	287.53	118.63	158.23
4	2	2	266.86	122.28	136.41
4	4	4	292.45	98.00	200.39
6	2	2	271.47	121.30	141.95
6	4	4	299.07	97.72	208.37
6	6	6	314.66	79.59	247.57
8	2	2	270.16	121.56	140.43
8	4	4	302.14	97.69	211.82
8	6	6	323.15	80.46	256.00
8	8	8	304.38	97.92	146.41
10	2	2	270.36	121.52	140.66
10	4	4	299.77	97.71	209.17
10	6	6	325.98	80.80	258.77
10	8	6	307.42	92.36	179.73
10	8	8	302.42	98.28	145.94

After the calculation of the Taylor coefficients, it is possible to apply the results on the GL criterion $P_{1,k_1} = P_{2,k_2} = P_{3,k_3} = 0$ for finding the critical endpoint. Using the Taylor polynomials leads to approximated values for the temperature, chemical potential and constituent mass. The system of equations is solved numerically by a variant of the secant method for different orders of the polynomials in a location of the exact critical endpoint. The obtained results are listed in table 4.2. First of all, one can see that the results are slightly varying for the choice of the Taylor orders, however, the rough position of the critical endpoint is already visible in the first line for an approach with order two for all coefficients. Moreover, it is clearly recognizable that the approximation improves stepwise for higher orders k_1 of the Taylor polynomial P_{1,k_1} . Then, again within a block the approach gets better by taking higher orders k_2 and k_3 . The biggest fluctuations compared to the exact solution triple is given by the values of the constituent masses M'_0 which are varying quickly in a range of 136.41 MeV to 258.77 MeV. The best solution for the constituent mass is given by $M'_0 = 179.73$ MeV through the Taylor

orders $k_1 = 10$, $k_2 = 8$ and $k_3 = 6$. For the temperature, the best solution is $T'_c = 80.80$ MeV by the the combination $k_1 = 10$ and $k_2 = k_3 = 6$. For the Taylor combination of $k_1 = 8$ and $k_2 = k_3 = 6$, one obtains the best approximation of the chemical potential with $\mu'_c = 323.15$ MeV. All in all, the results for solving the equation set 3.15 with $P_{1,10}$ and orders $k_2, k_3 \geq 4$ for the other polynomials lead to satisfying results for the CEP approach. Using these Taylor orders, the maximal distance of approximated and exact values is $\Delta\mu_c = 22.25$ MeV, $\Delta T_c = 16.09$ MeV as well as $\Delta M_0 = 72.16$ MeV which is less than a 20% deviation from the two relevant quantities μ_c and T_c . The best approximations for the critical temperature and chemical potential as tuple is obtained by $k_1 = 8, 10$ and $k_2 = k_3 = 6$ with $(323.15, 80.46)$ MeV and $(325.98, 80.80)$ MeV, respectively. Hence, these results of the Taylor series expansion fulfill the objective of this work and remain as a successful CEP approach.

4.2.1 Constituent mass functions for the Taylor polynomials

Next, one can have again a look on the behavior of the constituent mass functions for different Taylor orders at fixed temperatures. These plots reveal the information of the spinodals and CEP position due to the number of possible effective masses M_0 .

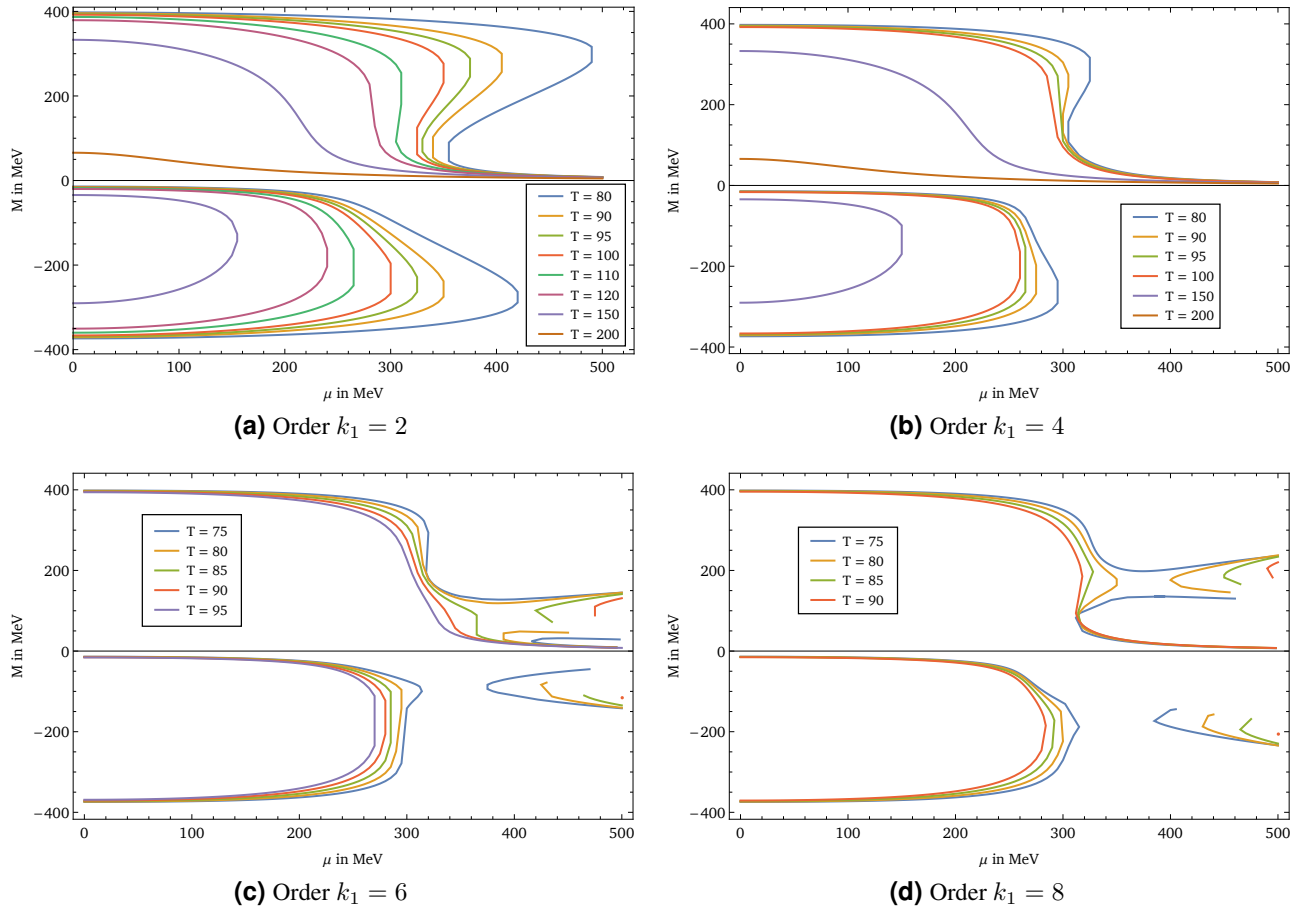


Figure 4.5: Constituent masses M as functions of the chemical potential for $m = 5.6$ MeV and different fixed temperatures T in MeV by the Taylor polynomials $P_{1,k_1}(T, \mu) = 0$ of order $k_1 = 2, 4, 6, 8$.

Therefore, one can already estimate the location of the CEP by analyzing the plots for different temperatures as it is done for the exact Ginzburg-Landau coefficient α_1 in figure 3.6. In this section, the equation $P_{1,k_1} = 0$ will be solved for M_0 for different orders k_1 of the Taylor polynomial and the results are depicted in figure 4.5. Low temperatures are not considered here because the approximation is bad in that case due to the evaluation around $\mu = 0$. The overall shape of the solution curves for the Taylor polynomials up to order two and four are similar to the exact ones in figure 3.6. One can see, how the shape transforms for higher temperatures to curves with only one positive constituent mass for every given chemical potential. Despite this, the transition from up to three possible solutions for M_0' to only one is shifted to higher temperatures and lies in the range between $T = 110$ MeV and $T = 120$ MeV for $P_{1,2}$. For the fourth Taylor polynomial of GL coefficient α_1 , one gets already an approximation of the CEP temperature between $T = 90$ MeV and $T = 95$ MeV just by analyzing the corresponding plot. For both Taylor approximations, the range for the chemical potential at the CEP is roughly given between $\mu = 260$ MeV and $\mu = 300$ MeV. Also, the behavior for high temperatures up to $T = 200$ MeV is similar to the exact case since the negative solutions vanish.

For the higher Taylor polynomials, it is more difficult and time-consuming to calculate solutions of the equation $P_{1,k_1} = 0$. Thus, the showed plots are more focused on the area of temperatures which are relevant for the CEP approximation. For order $k_1 = 6, 8$ there are additional solutions for the constituent mass in the positive and negative area for high chemical potentials. These solutions have not a perfect resolution but one can see the general behavior. Nevertheless, one has to keep in mind that the kinks in the curves of the order $k_1 = 8, 10$ solutions have their origin in the calculation, where not as much points could be computed as for lower orders or in the exact case. Clearly, it is a big disadvantage of the higher orders, that additional solutions come up for the constituent masses due to extra zeros in the course of the $P_{1,k_1}(M)$ function. The general behavior of the first two orders fits better to the exact calculation in figure 3.6. However, searching again the area of the approximated CEP gives a range between $T = 75$ MeV and $T = 85$ MeV and $\mu = 300$ MeV till $\mu = 320$ MeV for the sixth order as well as a range between $T = 85$ MeV and $T = 90$ MeV and again $\mu = 300$ MeV till $\mu = 320$ MeV for Taylor order $k_1 = 8$. These results are closer to the exact value for both, the temperature and the chemical potential, although the course of the solution curves is more different to the exact case. Hence, it was possible to find already an approximated range for the CEP values by analyzing the constituent mass functions for the Taylor polynomials.

5 Conclusion and outlook

This work focused on the determination of the position of the critical endpoint and tricritical point in the QCD phase diagram for a simplified two-flavor Nambu-Jona-Lasinio model [7]. Therefore, first the NJL Lagrangian was considered before the thermodynamic potential Ω_{NJL} was derived in mean-field approximation. The behavior of the grand potential for different points in the phase diagram was depicted in the figures 2.5 and 2.4 where the chiral symmetry is clearly visible and the phase boundaries can be imagined by the change of the stationary points. Together with the gap equation 2.11 the possible constituent mass solutions could be investigated in the chiral limit and for nonzero current quark mass in figure 2.6. It was worked with the parameter set 2.29 and $m = 5.6$ MeV since a sharp 3-momentum cut-off was necessary due to the occurrence of divergent integrals.

In the next step, the Ginzburg-Landau theory was introduced as method to describe and analyze phase transitions through expanding the grand potential Ω_{NJL} in an order parameter field M around a solution M_0 of the gap equation in relation 3.4. An analysis of the sign restriction for the Ginzburg-Landau coefficients α_n at different points in the phase diagram and on the boundary led to two conditions for calculating the exact position of TCP and CEP [15]. In the chiral limit, the TCP can be determined by solving $\alpha_2(T, \mu) = \alpha_4(T, \mu) = 0$ and for the critical endpoint in the case of finite bare masses the solution of $\alpha_1(T, \mu) = \alpha_2(T, \mu) = \alpha_3(T, \mu) = 0$ is needed. Solving these systems of equations numerically with Newton and secant methods leads to the exact tricritical point with $T_{TCP} = 112.78$ MeV and $\mu_{TCP} = 266.04$ MeV as well as to the exact critical endpoint at $m = 5.6$ MeV with values $T_{CEP} = 82.19$ MeV, $\mu_{CEP} = 322.02$ MeV and $M_{CEP} = 186.61$ MeV. Moreover, the exact phase diagrams with spinodals and first as well as second order phase boundary in the chiral limit could be calculated and the results were shown in the figures 3.2 and 3.5. The approximate position of the TCP and CEP as well as the spinodals are already apparent from the plots of the constituent mass functions in the figures 3.3 and 3.6.

The main purpose of this work is the approach of the critical points through applying Taylor series expansions as it was already done in [18] for the pressure p . Since the results in [18] were not satisfactory, the idea of expanding another quantity come up, such that the Ginzburg-Landau coefficients were used for an expansion with respect to μ . The evaluation point $\mu = 0$ is based on the fact that Taylor expansions of certain quantities around $\mu = 0$ are also possible in lattice QCD. Starting in the chiral limit with trivial solution $M = 0$, it was possible to derive an exact polynomial expression of second order for the α_2 coefficient in equation 4.3. The fourth GL coefficient was expanded to order $k = 34$ and this led to nearly the exact TCP values. However, the expansion up to order $k = 10$ gave already a satisfactory approximation with $T'_{TCP} = 116.71$ MeV and $\mu'_{TCP} = 260.40$ MeV. The situation for the finite mass $m = 5.6$ MeV was much more complicated since Tay-

lor series expansions for the first three coefficients were needed and the evaluation point for the coefficients α_2 and α_3 is a nontrivial solution M_0 of the gap equation. Nevertheless, an expansion up to order $k_1 = 8, 10$ for the first coefficient allowed a satisfactory approximation of the CEP, especially by using the Taylor expansion up to order $k_2 = k_3 = 6, 8$ for the other coefficients. The best result is therefore through Taylor orders $k_1 = 8$ and $k_2 = k_3 = 6$ with values $T'_{CEP} = 80.46$ MeV and $\mu'_{CEP} = 323.15$ MeV but a little bit less good result for the constituent mass $M'_0 = 256$ MeV which is varying quickly in the region around the CEP. Going to higher orders for α_2 and α_3 improves the constituent mass solution but decreases the quality for potential and temperature approximation.

Finally, the Taylor series expansion of the Ginzburg-Landau coefficients allows an estimation of the critical points. These approximations can be improved by calculating higher Taylor orders and the NJL model should include vector interactions as well as a third quark flavor and non-degenerate quark masses. It remains to investigate the situation for different parameter sets and other finite bare masses than $m = 5.6$ MeV. Hopefully, the quality of the approaches will be similar to the approximations of this work. If this also leads to a good estimation of the CEP, one could think about a comparable quantity for lattice QCD to proceed such a Taylor expansion around $\mu = 0$. Actually, it is not clear which quantity could correspond to the Ginzburg-Landau coefficients but all in all, the results are much better than Taylor expansions of physical quantities like the pressure p in [18]. Nevertheless, the approaches of lattice QCD and NJL model are very different.

Bibliography

- [1] G. Ecker: *Quantum Chromodynamics*, Lectures given at the 2005 European School of High-Energy Physics, 2006, arXiv:hep-ph/0604165
- [2] M. Durante et al.: *All the Fun of the FAIR: Fundamental physics at the Facility for Antiproton and Ion Research*, Physica Scripta 94, 033001, 2019, arXiv:1903.05693
- [3] Y. Nambu, G. Jona-Lasinio: *Dynamical Model of Elementary Particles Based on an Analogy with Superconductivity. I.*, Phys. Rev. 122, 345-358, 1961
- [4] Y. Nambu, G. Jona-Lasinio: *Dynamical Model of Elementary Particles Based on an Analogy with Superconductivity. II.*, Phys. Rev. 124, 246-254, 1961
- [5] S. P. Klevansky: *The Nambu-Jona-Lasinio model of quantum chromodynamics*, Rev. Mod. Phys. 64, 649-708, 1992
- [6] S. Vereeken: *Chiral Symmetry Breaking Phases at High Chemical Potential in the Nambu-Jona-Lasinio Model*, Bachelor thesis, Technische Universität Darmstadt, 2015
- [7] M. Buballa: *NJL-model analysis of dense quark matter*, Phys. Rep. 407, 205-376, 2005, arXiv:hep-ph/0402234v2
- [8] P. Schmüser: *Feynman-Graphen und Eichtheorien für Experimentalphysiker*, 2nd edition, Springer-Verlag, Berlin, 1995
- [9] M. Peskin, D. Schroeder: *An Introduction To Quantum Field Theory*, Westview Press, New York, 1995
- [10] J. Kapusta, C. Gale: *Finite Temperature Field Theory: Principles and Applications*, 2nd edition, Cambridge University Press, New York, 2006
- [11] J. Hirsch: *Mesonic Excitations in an Inhomogeneous Phase of the Nambu-Jona-Lasinio Model*, Master thesis, Technische Universität Darmstadt, 2013
- [12] F. Schwabl: *Statistische Mechanik*, 3rd edition, Springer-Verlag, Heidelberg, 2006
- [13] T. Fließbach: *Statistische Physik*, 6th edition, Springer Spektrum, Berlin, 2018
- [14] P. Hohenberg, A. Krekhov: *An introduction to the Ginzburg-Landau theory of phase transitions and nonequilibrium patterns*, Phys. Rep. 572, 1-42, 2015, arXiv:1410.7285v3

-
-
- [15] M. Buballa, S. Carignano: *Inhomogeneous chiral phases away from the chiral limit*, Phys. Lett. B791, 361-366, 2019, arXiv:1809.10066v3
- [16] M. Buballa, S. Carignano: *Influence of quark masses and strangeness degrees of freedom on inhomogeneous chiral phases*, PoS, XIII Quark Confinement and the Hadron Spectrum - Confinement 2018, Maynooth University, Ireland, 2018, arXiv:1906.03241v1
- [17] C. R. Allton, M. Döring, S. Ejiri, S.J. Hands, O. Kaczmarek, F. Karsch, E. Laermann, K. Redlich: *Thermodynamics of two flavor QCD to sixth order in quark chemical potential*, Phys. Rev. D71, 054508, 2005
- [18] D. Scheffler: *NJL model study of the QCD phase diagram using the Taylor series expansion technique*, Bachelor thesis, Technische Universität Darmstadt, 2007

Erklärung zur Abschlussarbeit gemäß §23 Abs. 7 APB der TU Darmstadt

Hiermit versichere ich, Robin Alexander Beck, die vorliegende Bachelor-Thesis ohne Hilfe Dritter und nur mit den angegebenen Quellen und Hilfsmitteln angefertigt zu haben. Alle Stellen, die Quellen entnommen wurden, sind als solche kenntlich gemacht worden. Diese Arbeit hat in gleicher oder ähnlicher Form noch keiner Prüfungsbehörde vorgelegen.

Mir ist bekannt, dass im Falle eines Plagiats (§38 Abs.2 APB) ein Täuschungsversuch vorliegt, der dazu führt, dass die Arbeit mit 5,0 bewertet und damit ein Prüfungsversuch verbraucht wird. Abschlussarbeiten dürfen nur einmal wiederholt werden.

Bei der abgegebenen Thesis stimmen die schriftliche und die zur Archivierung eingereichte elektronische Fassung überein.

Thesis Statement pursuant to §23 paragraph 7 of APB TU Darmstadt

I herewith formally declare that I, Robin Alexander Beck, have written the submitted thesis independently. I did not use any outside support except for the quoted literature and other sources mentioned in the paper. I clearly marked and separately listed all of the literature and all of the other sources which I employed when producing this academic work, either literally or in content. This thesis has not been handed in or published before in the same or similar form.

I am aware, that in case of an attempt at deception based on plagiarism (§38 Abs. 2 APB), the thesis would be graded with 5,0 and counted as one failed examination attempt. The thesis may only be repeated once.

In the submitted thesis the written copies and the electronic version for archiving are identical in content.

Ort/Place, Datum/Date

Unterschrift des Autors/Signature of author